Bachelor Thesis BMT

FABRICATION AND CHARACTERIZATION OF AN OPTICALLY STABLE TISSUE PHANTOM FOR THE EVALUATION OF TRANSCUTANEOUS BILIRUBIN METERS

April 25, 2024

Author:

Anna Karreman

Bachelor Thesis committee:

prof.dr.ir. N. Bosschaart

ir. A.J. Dam – Vervloet

prof. dr. S. Manohar

UNIVERSITY OF TWENTE.

1 ABSTRACT (ENGLISH)

This thesis focuses on the fabrication and characterization of an optically stable tissue phantom for the evaluation of transcutaneous bilirubin meters (TcB meters), a crucial tool in diagnosing neonatal jaundice in a non-invasive way. Neonatal jaundice, resulting from hyperbilirubinemia, is a common condition among newborns that can lead to severe complications if left untreated. While TcB measurements offer a non-invasive approach to estimate bilirubin levels, their accuracy can be influenced by several factors, including the optical properties of neonatal skin. This research aims to fabricate a phantom that accurately mimics the optical properties of neonatal skin for the evaluation of TcB-meters.

By analyzing the absorption and scattering properties of various yellow, magenta, and white acrylic paint pigments mixed with epoxy resin, phantoms were fabricated mimicking different TcB concentrations. The optical properties of the fabricated phantoms were analyzed using Collimated Transmission and afterwards tested with TcB-meters using different experimental protocols. The results from these measurements demonstrate that these phantoms can effectively replicate the optical properties of jaundiced neonatal skin. Future research should focus on optimizing the experimental protocol, to minimize the variability of the TcB measurements. Furthermore, the stability of the phantoms over an extended period of time should be evaluated.

1 ABSTRACT (NEDERLANDS)

Deze bachelor opdracht richt zich op het fabriceren en karakteriseren van een optisch stabiel weefstelfantoom voor de evaluatie van transcutane billirubinemeters (TcB-meters), een cruciaal instrument voor de diagnose van neonatale geelzucht op een niet-invasieve manier. Neonatale geelzucht, voortkomend uit hyperbilirubinemie, is een veelvoorkomende aandoening bij pasgeboren baby's met ernstige gevolgen indien onbehandeld. Hoewel TcB-metingen een niet-invasieve benadering bieden om bilirubineniveaus te schatten, kan hun nauwkeurigheid worden beïnvloed door verschillende factoren, waaronder de biologische variatie in de optische eigenschappen van huid.

Dit onderzoek heeft als doel om een fantoom te fabriceren dat de optische eigenschapen van neonatale huid nauwkeurig nabootst en daarmee TcB-meters evalueert.

Door de absorptie- en verstrooiingseigenschappen van verschillende gele, magenta en witte acrylverfpigmenten gemengd met epoxyhars te analyseren, werden fantomen gefabriceerd die verschillende TcB-concentraties nabootsen. De optische eigenschappen van de gefabriceerde fantomen werden geanalyseerd met behulp van gecollimeerde transmissie en vervolgens getest met TcB-meters met verschillende meetprotocollen. De resultaten van deze metingen tonen aan dat deze fantomen effectief het optische gedrag van bilirubine in neonatale huid kunnen repliceren. Toekomstig onderzoek zou zich kunnen richten op het optimaliseren van het meetprotocol, om de variabiliteit van de TcB-metingen te minimaliseren. Verder moet de stabiliteit van de fantomen over een langere periode worden geëvalueerd.

2 TABLE OF CONTENTS

3 INTRODUCTION

3.1 HYPERBILIRUBINEMIA

Hyperbilirubinemia is a common clinical condition in newborn infants and is caused by an elevated total serum bilirubin (TSB).[1] Bilirubin is a naturally occurring yellow compound and a breakdown product of hemoglobin.[2] Most of the bilirubin in blood is bound to albumin in a water-soluble bilirubin-albumin complex. However, when the bilirubin-albumin binding capacity is exceeded, small amounts of unbound bilirubin leave the intravascular space, resulting into an elevated amount of bilirubin in skin tissue. Jaundice is a sign of hyperbilirubinemia and appears as a yellow skin tone and sclerae. The term jaundice derives from the French word “jaune”, which means yellow.[3]

An excess of bilirubin is common in newborn infants in the first week after birth, due to immature liver functioning and an extra breakdown of red blood cells. Approximately 60% of term and 80% of preterm newborns develop some degree of jaundice in the first week after birth.[1] Most cases of hyperbilirubinemia are harmless. Nevertheless, high bilirubin concentrations may result in acute irreversible brain damage, also called kernicterus. Kernicterus is a permanent neurological condition, which may induce hearing loss and deafness, developmental disabilities, motor impairments and abnormal enamel on teeth.[4] Therefore, careful monitoring of high-risk newborn infants is essential.

3.2 DIAGNOSIS

Jaundice is commonly measured with two different approaches. The conventional approach for measuring bilirubin is a TSB determination from a blood sample obtained by invasive blood sampling. Although successful in preventing kernicterus, the method has limitations. Invasive blood sampling causes discomfort and stress for the neonate, leading to higher potential risk for osteomyelitis and infections at the sampling site. Furthermore, the method is laborious and time consuming, limiting the possibility for fast diagnosis and bedside monitoring.[4,5] Since the measurement of bilirubin levels plays a significant role in diagnosis and prognosis of jaundice, a more timely and non-invasive treatment method is crucial.[3]

Transcutaneous bilirubinometry offers a non-invasive, pain-free alternative, providing immediate results without the need for invasive blood sampling. The technique is based on optical spectroscopy, relating the concentration of bilirubin in the skin to the amount of light absorbed by bilirubin in the skin. [5] This technique can be used to decrease the number of invasive TSB measurements. However, transcutaneous bilirubinometry cannot completely replace TSB measurements, due to the fundamental physiological differences between the TSB and TcB. Specifically, the TSB comprises the

bilirubin concentration in intravascular space, whereas the TcB mainly reflects the contribution of extravascular bilirubin.[4,5] In addition, measured TcB values may vary depending on infant's skin pigmentation and postnatal age, limiting a consistent and fully accurate measurement of bilirubin concentrations.[6] This leads to a spread of ±40 μmol/L around the measured TcB concentration, ranging from 0 to 400 μmol/L.[7] Due to this inaccuracy of the TcB, a clinically accepted safety margin of 50 µmol/L is commonly used around the measured TcB.[3] Clinical guidelines currently recommend performing an additional blood test for TSB analysis if the TcB exceeds the TSB therapy threshold within this safety margin. The TSB therapy threshold depends on various risk factors associated with the neonate's health status (e.g. hemolytic disorders, lowered Albumin levels <30 g/L, suspicion of infection or sepsis or if a neonate seems lethargic[8]), weight and (gestational) age. [9]

3.2.1 Working principle of transcutaneous bilirubinometry

As mentioned earlier, transcutaneous bilirubinometry is based on optical spectroscopy and relates the optical absorption of bilirubin in the skin to its concentration. Commonly used TcB meters, like JM-105 from Dräger, emit light with wavelengths of 450 nm and 550 nm, in the blue and green wavelength region, respectively. The emitted light is directed to the skin via a bundle of fibers and utilizes two optical pathways: a shorter optical path that is used to evaluate the skin's most superficial tissue layers and a longer pathway that provides insight into the deeper (sub)cutaneous tissue. The green and blue photons that scatter back from the skin are captured by a set of fibers designed for detection.[10] The working principle of the bilimeter is visualized in Figure 1. Bilirubin specifically absorbs light around 450 nm, referred to as the bilirubin absorption peak, while hemoglobin absorbs light at both 450 nm and 550 nm. Therefore, the bilimeter attempts to correct the presence of chromophores other than bilirubin by measuring the absorption at 450 nm and correcting for the background absorption at 550 nm. In practice, most bilimeters are designed to be used on the forehead and sternum of the infant.[3,10]

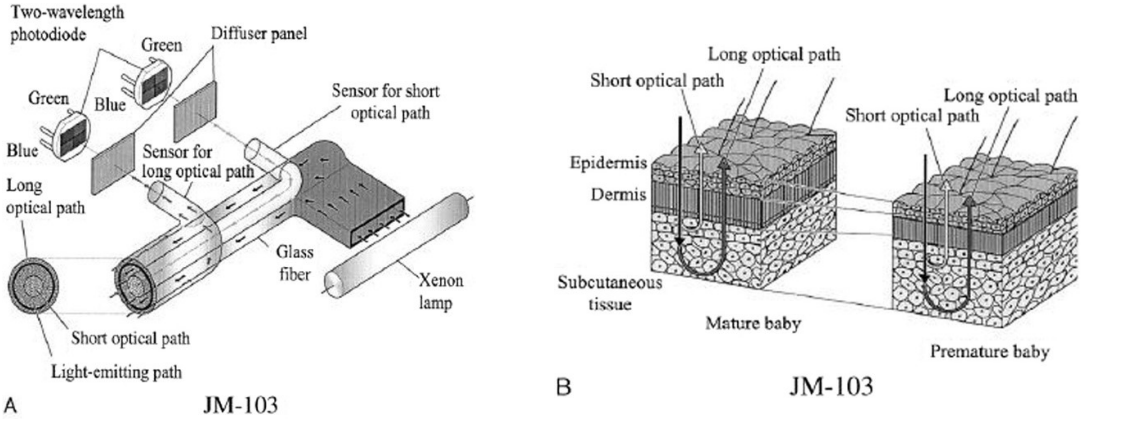

Figure 1: *The working principle of transcutaneous bilirubinometry (Dräger JM-105) itself (A) and the skin (B)*[10]

3.3 OPTICAL PROPERTIES OF NEONATAL SKIN

The transfer of light inside skin depends on the absorption and scattering properties of the structures and molecules in the skin.[3] Absorption is quantified by the absorption coefficient μ_a (m^{-1}). The reciprocal of μ_a, $1/\mu_a$, represents the average path length traveled by a photon before it is absorbed. In the visible wavelength range, hemoglobin, bilirubin, and melanin are the primary absorbing molecules (i.e. chromophores) in the neonatal skin. The corresponding absorption spectra are shown in Figure 2.

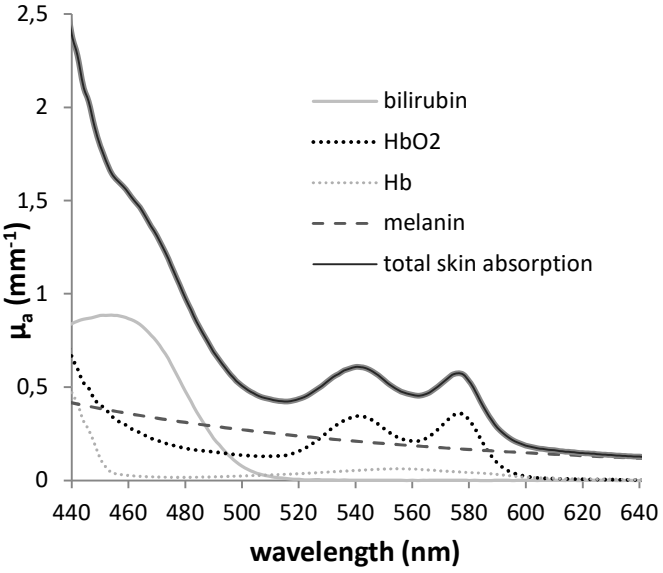

Figure 2: *Absorption spectrum of the most significant skin chromophores in the visible wavelength range for a hemoglobin concentration of 2.13 g/L and bilirubin concentration of 70µmol/L.* [11]

Light scattering, on the other hand, occurs when photons change their original direction and is described by the scattering coefficient μ_s (m^{-1}). The reciprocal of μ_s, $1/\mu_s$, represents the average path length traveled by a photon before it is scattered. The total attenuation μ_t, which describes the total reduction of intensity of light, is therefore defined as the sum of μ_s and μ_a. The scattering anisotropy, denoted as *g*, quantifies the average cosine of the scattering angle. The value of g ranges between -1 and 1, with g = 1 describing purely forward scattering, g = -1 describing purely backward scattering and g = 0 describing isotropic scattering (scattering in all directions). The reduced scattering coefficient, μ_s', incorporates this anisotropy factor into μ_s as follows:

$$\mu_s' = \mu_s(1 - g) \tag{1}$$

The optical properties of neonatal skin can vary due to differences in skin composition, like bilirubin, melanin and hemoglobin concentration in the skin, skin maturity and skin pigmentation. [3] The corresponding optical properties have comprehensively been studied in literature, in which the results

varying among studies. Figure 3 displays the optical properties of neonatal skin at the sternum and forehead studied by Bosschaart et al. (2011), showing the spread of optical properties among a group of 60 preterm newborns.[7]

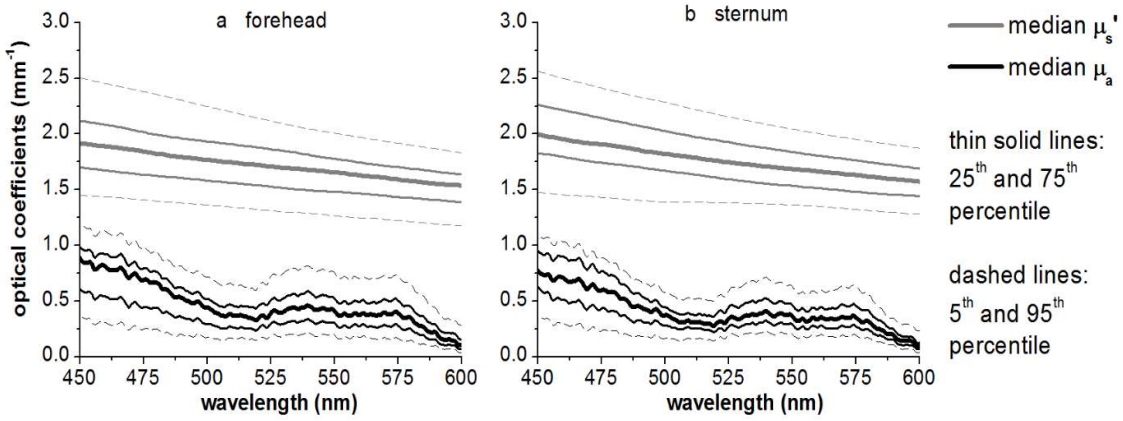

Figure 3: *Optical properties of the neonatal skin for a) forehead and b) sternum. Figure adapted from Bosschaart et. al (2011)* [7]

Dam Vervloet et al. (2024) used the optical properties in Figure 3 to design a series of optical phantoms that mimic a range of bilirubin concentrations in neonatal skin, as shown in Table 1. The absorption coefficient at 550 nm was kept constant to mimic a stable hemoglobin concentration of 2.13 g/L, which is the average value for neonatal skin. The mimicked TcB corresponds to the average measured TcB value by the Dräger JM-105 bilimeter of five measurements through a plain Tegaderm™ film.[12]

Table 1: *Phantoms from the study by Dam-Vervloet et al. with different mimicked TcB values and their corresponding optical properties.*[13]

Mimicked TcB value (µmol/L)	**Corresponding μ_a (mm^{-1})**	
	450 nm	550 nm
0	0.50	0.32
22	0.65	0.32
87	1.09	0.32
145	1.74	0.33
172	2.21	0.33
198	2.70	0.33
222	3.25	0.34
238	3.97	0.34
249	4.49	0.35

Furthermore, the reduced scattering coefficient of these phantoms are 2.00 mm^{-1} at 450 nm and 1.63 mm^{-1} at 550 nm, which approximate the average values for neonatal skin, as displayed in Figure 3.[7]

3.4 PHANTOM DESIGN AND STABILITY

For the evaluation of the performance of a device in medical imaging and sensing, the use of phantoms with known optical properties is essential.[14] Optical tissue phantoms typically consist of three components: a matrix material, an absorbing agent, and a scattering agent. An ideal phantom can be used for all applications and optical modalities. This requires a solid phantom with tunable optical properties over a broad spectral range, while being stable over time and throughout multiple uses. In addition, there should be full control over the geometry of the phantom.

Optical properties of phantoms can be constructed by directly using biological chromophores, such as whole blood or hemoglobin. While these phantoms give accurate results, the shelf life of these phantoms ranges between a few hours and a couple of weeks. To create phantoms with optical properties that remain constant over a longer period of time, materials like silicone or resin are chosen for their transparency and resistance to environmental changes, ensuring a longer shelf life. However, the use of these stable, inorganic materials is incompatible with the use of biological chromophores, preventing them from easily matching the spectral optical properties of tissue. Alternatively, the optical properties of phantoms with a matrix of inorganic materials are controlled through the addition of pigments and powders, to provide scattering and absorption across the spectrum. Adjusting the

concentration of these added substances makes it possible to achieve almost any combination of absorption and scattering coefficients at a specified wavelength.[15]

While previously fabricated optical phantoms successfully mimic certain concentrations of TcB, a significant problem remains the stability of these phantoms over longer periods of time. This lack of stability prevents longitudinal evaluation of TcB meter performance. Therefore, an optical phantom is needed that not only accurately replicates the optical properties of biological tissue, but also remains consistent over time and repeated use.

3.5 AIM OF THE THESIS

The aim of this thesis is to develop an optically stable phantom, with an optimal minimal shell life of 6 months, that mimics both the optical absorption and scattering properties of neonatal skin at a wavelength of 450 nm and 550 nm.

4 MATERIALS AND METHODS

4.1 PHANTOM DESIGN AND FABRICATION

4.1.1 Component Selection

As mentioned earlier, optical tissue phantoms typically consist of three basic components: a matrix material, an absorbing agent, and a scattering agent. The desired phantom for this thesis should meet at least the following requirements:

- The phantom absorption at 450 nm and 550 nm should be independently tunable, matching the absorption contribution of bilirubin and hemoglobin to the optical properties of neonatal skin. This implies a tunable absorption range of 0.5 to 4.5 mm^{-1} at 450 nm and a tunable absorption range of 0.3 to 0.4 mm^{-1} at 550 nm.
- The phantom scattering properties at 450 and 550 nm should match the average reduced scattering properties of neonatal skin. This implies a reduced scattering coefficient of approximately 2.00 mm^{-1} at 450 nm and 1.63 mm^{-1} at 550 nm.
- The phantom must have high optical stability over time, i.e., the optical properties of the phantom should be independent of shelf life for at least six months.

In addition to these requirements, the phantom should preferably be easy to fabricate, using accessible components and remain low cost. As a first step, a literature search was performed for studies that describe fabrication procedures of phantoms that potentially match the criteria listed above. Table 2 presents an overview of these studies.

Table 2: *Comparison of different phantoms from different studies, judging their usability for bilirubin and hemoglobin measurements.*

Study	Matrix	Scattering agent	Absorption agent	(Independently) tunable absorption at 450 nm?	(Independently) tunable absorption at 550 nm?	Stability
Lualdi et al. (2001) [14]	High-stretch two-component room-temperature curing silicone (Elastosil RT 604)	Cosmetic powder and Al_2O_3 particles. The study does not measure μ_s directly, but total attenuation, which ranges from 170 to 190 mm^{-1}.	Cosmetic powder (Cream Powder, Deep Beiger, Max Factor, UK)	Yes, μ_a is independently tunable from 0 to 4 cm^{-1}.	Yes, μ_a is independently tunable from 0 to 2.5 cm^{-1}.	Due to the silicone matrix, the study suggests the phantom to be stable over time.
Zhou et al. (2012) [2]	5% gelatine (G1890, Sigma-Aldrich)	1% Intralipid (Fresenius Kabi) is used and has a scattering coefficient of approximately 1000 mm^{-1}.	Bilirubin powder (B4126, Sigma-Aldrich) dissolved in dimethyl sulfoxide and Lysed bovine blood with 75% sO_2 (905-250, Quad Five)	Yes. However, the range of μ_a is not given.	Yes, μ_a is tunable by varying concentrations of bilirubin powder with a μ_a of 50 mm^{-1} M^{-1} $x10^4$	There is no mention on the stability of the phantom.
Veenstra et al. (2018) [16]	Aqueous solution in combination with a thin silicone layer.	Polystyrene spheres (400 nm diameter, Thermo Scientific USA) and a silicone layer containing 0.1% TiO_2, mimicking the upper part of the neonatal dermis. A scattering coefficient of 9 mm^{-1} was mimicked.	Bilirubin (Sigma-Aldrich, Germany) made soluble in Dimethyl Sulfoxide and adjusted to the desired concentration.	The phantom is specifically designed for testing bilirubin, so this phantom can effectively mimic the interaction of light with bilirubin, with an approximate tunable attenuation coefficient range of 12 to 16 mm^{-1}	The phantom has an approximate attenuation coefficient range of 5 to 7 mm^{-1}. However, the phantom is not independently tunable, since only one absorbing agent is used.	There is no mention in the article on the stability of the phantom.
Van Erk et al. (2019) [12]	Aqueous solution measured through a transparent Tegaderm film dressing.	Light scattering was mimicked using Intralipid (20% Fresenius Kabi, Bad Homburg, Germany). The study has different phantom designs, with reduced scattering coefficient ranging from 1.36 to 2.27 mm^{-1}.	The total skin absorption by bilirubin and hemoglobin was mimicked by individual tuning of two dyes (Ecoline: Light-Yello-201 and Magenta-337, Royal Thalens, The Netherlands)	Yes, the study has different phantom designs specifically measured at 450 nm, with μ_a ranging from 1.02 to 2.12 mm^{-1}.	Yes, the study has different phantom designs specifically measured at 550 nm, with μ_a ranging from 0.01 to 0.35 mm^{-1}.	There is no mention in the article about the stability of the phantom.

Study	Matrix	Scattering agent	Absorption agent	(Independently) tunable absorption at 450 nm?	(Independently) tunable absorption at 550 nm?	Stability
Ntombela et al. (2020) [17]	Tryptone soy and Bacteriological Agar powder (Sigma Aldrich, MO, USA).	Aluminium oxide particles (64271, Darmstadt, Germany). In the study the scattering coefficient was ranged from 5,4 to 14,2 mm^{-1}.	India ink (PRO-4100, Pro Art)	The study does not specifically measure at a wavelength of 450 nm.	No, μ_a is not independently tunable. In the study μ_a ranged from 4,8 to 14,2 mm^{-1}.	The stability of these phantoms was confirmed over 30 days of storage at 21 degrees.
Sieryi et al. (2020) [18]	Polyvinyl chloride-plastisol (PVCP)	ZnO or TiO_2 particles. At a wavelength of 900 nm, the reduced scattering coefficient is equal to 1.5 mm^{-1} for a skin phantom.	A black pigment (CI Pigment Black 7 ink from M-F Manufacturing)	No, μ_a is not independently tunable. The study shows a range of absorption coefficient from 0.05 to 0.22 mm^{-1} at a wavelength of 900 nm, depending on concentration. There is no mention of bilirubin in the article.	No, μ_a is not independently tunable. The study shows a range of absorption coefficients from 0.05 to 0.22 mm^{-1} at a wavelength of 900 nm, depending on concentration. The article does however compare the phantom to hemoglobin and blood.	When the phantom is stored in a vacuumchamber, it shows great stability over 30 days.
	Polydimethylsiloxane (PDMS) forms a silicone base	Spherical cavities within the silicone matrix filled with glycerol that are naturally formed in the silicone matrix.	No other absorbers were used, and the intrinsic absorption property of the matrix is used.	No, the phantom is not tunable at 450 nm.	No, the phantom is not tunable at 450 nm.	When the phantom is stored in a vacuumchamber, it shows great stability over 30 days.
Walter and Jansen (2023) [15]	JANCHUN Crystal Clear Epoxy Resin Kit	Titanium dioxide, Zincoxide and Al_2O_3 in acrylic paint form. The reduced scattering coefficient has a range of 0 to 3 mm^{-1}.	Yellow and magenta acrylic paints.	Yes, μ_a is independently tunable with μ_a ranging from 0,1 to 0,6 mm^{-1} per milligram of pigment per gram of matrix.	Yes, μ_a is independently tunable with μ_a ranging from 0 to 0,4 mm^{-1} per milligram of pigment per gram of matrix.	According to the ASTM standard test methods, which evaluates the degree in change of color when exposed to light, all the pigments have high stability over time and usage.

Even though several studies match one or more requirements, the phantom made in the study from Walter and Jansen is the only study to meet all the requirements and preferences:

- The phantom absorption is independently tunable at both 450 and 550 nm. Since the study defines the absorption coefficient as mm^{-1} per milligram of pigment per gram of matrix, the phantoms are easily reproducible for different concentrations.
- There is a separate scattering coefficient, with almost no absorption, which makes it possible to tune the phantom scattering independently from the phantom absorption.
- The pigments selected for the phantom are chosen specifically for their stability over time and usage, suggesting that, in combination with the epoxy resin, the phantom could have a shelf-life of at least several years.
- The pigments and matrix materials used are easy to fabricate using accessible and low-cost components.

Therefore, Walter and Jansen's study is most suitable for this thesis and the method used to reproduce this phantom is directly adapted from their study. The specific acrylic paint pigments that were chosen to characterize for this thesis are shown in Table 3. The choice of the pigments is based on the absorption and scattering coefficients at both 450 and 550 nm, displayed in Figure 4.

Table 3: *Absorbing and scattering pigments used in the phantom.*

Pigment	Brand	Color name
Absorbing agents		
PY65	Winsor & Newton: Galeria acrylic	Cadmium yellow deep hue
PY74	Liquitex: Basics acrylic	Primary yellow
PR122	Golden: Heavy body acrylics	Quinacridone magenta
PR170	Winsor & Newton: Galeria acrylic	Crimson
Scattering agents		
PW6	Plaza Art: Artists' acrylic	Titanium white

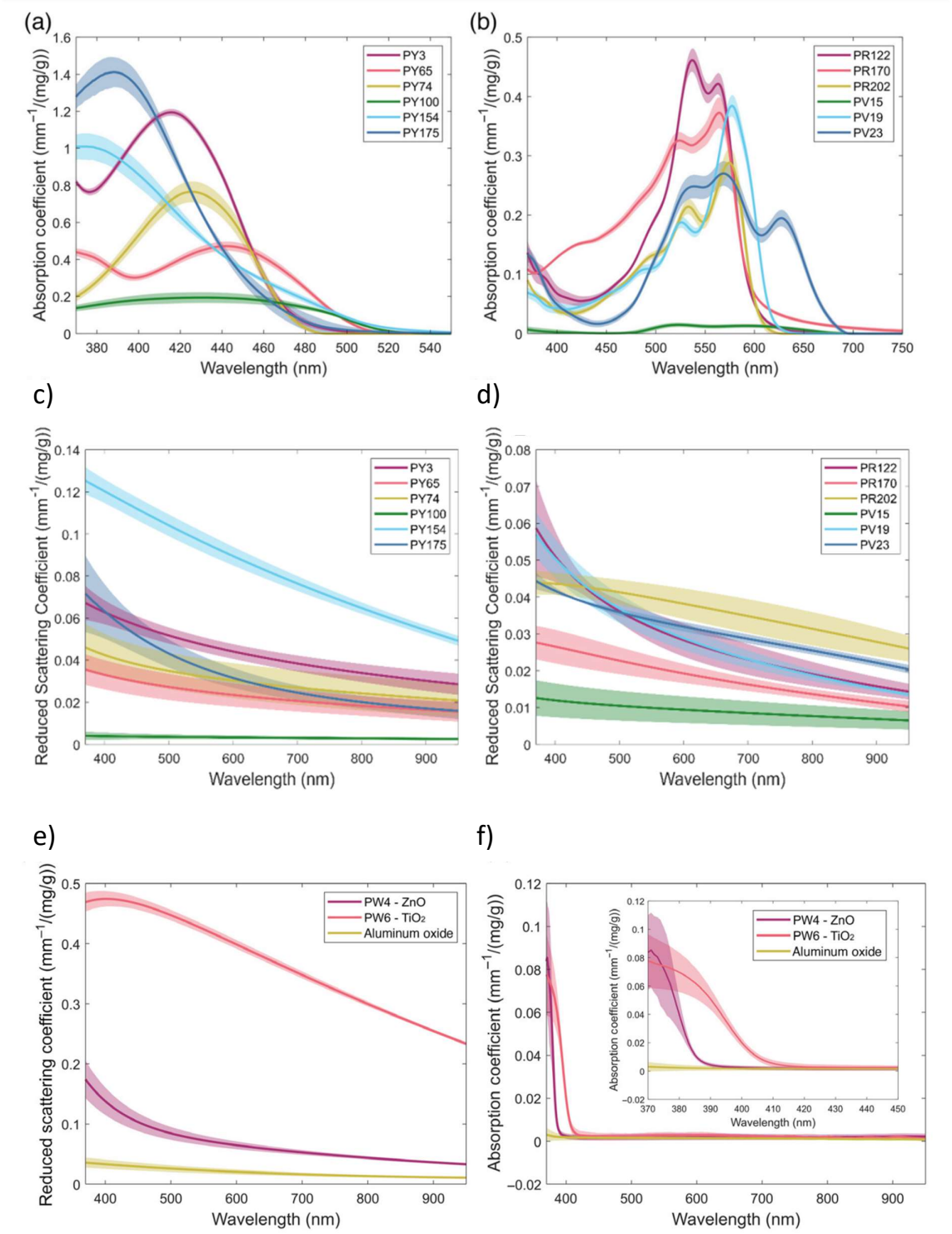

Figure 4: *The absorption spectra of a) the yellow pigments, b) the magenta pigments, f) white pigments, and reduced scattering coefficients of c) the yellow pigments, d) the magenta pigments, e) white pigments characterized in Walter and Jansen (2023). Pigments PY74, PY65, PR122, PR170 and PW6 were selected for this thesis. Figure adapted from Walter and Jansen (2023)* [15]

For the matrix material, a two-part epoxy resin (JANCHUN Crystal Clear Epoxy Resin Kit) is used. This matrix meets the criteria by having inexpensive material cost, relatively quick cure time and high stability over time. The epoxy resin consists of a base material (part A) and a hardener (part B), which are mixed using a 1A:0.9B weight ratio. The epoxy will fully cure after 24 hours at room temperature, but can still be manipulated the first 30 to 40 minutes after mixing. To minimize the risk of any additives settling during the cure time, the curing time can be reduced to approximately 30 min by elevating the temperature to 70 °C.

4.1.2 Phantom Fabrication

The phantom fabrication procedure described next has been adapted from the study of Walter and Jansen[15]. At first, the desired quantities of the yellow and magenta pigments are weighted. Next, water weighing approximately 10% of the desired mass of part A epoxy is added to rehydrate and dilute the acrylic paints. This is mixed using a glass stir rod until the color is homogenous. Following this, the mixture is put back on the analytical balance and the desired amount of part A epoxy is weighed and mixed by hand with the thinned pigments until a smooth emulsion is achieved. Since the water was only added to ensure the fabrication of a homogenous solution, the excess water should be removed. To remove the added water, the emulsion is placed in a vacuum chamber and subjected to -750 mmHg of pressure until the bubbles stop forming. This process is then repeated in a separate container to combine part B of the epoxy with the white pigment. This time at least 30% more water should be added compared to the weight of the white pigments.

After removing the water of both mixtures, the part A mixture is poured into the part B one and mixed by hand until it becomes a homogeneous mixture. Then an initial degassing is performed by placing the mixture into a vacuum chamber and brining the pressure to -750 mmHg until the bubbles stop forming or if 10 minutes have passed. It is important to use a large enough vessel, since resin expands by a large degree during degassing. Subsequently, the epoxy mixture is poured into silicone molds, ensuring a smooth surface of the phantom. The silicone mold is round with a diameter of 6 cm and a thickness of 1,5 cm. In addition to that, a small portion of the mixture is placed between two microscope plates, separated by two microscope plates, functioning as spacers, visualized in Figure 5a.

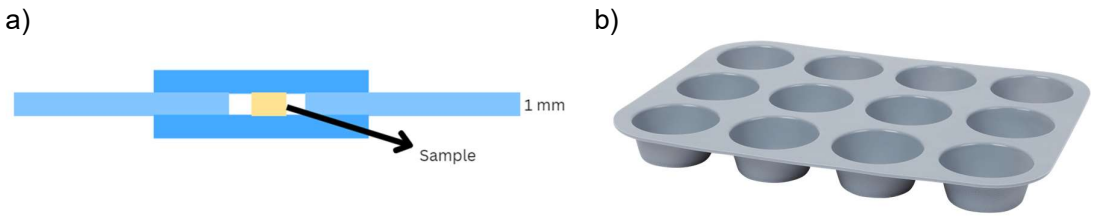

Figure 5: *a) Visualization of the setup for creating thin layers of the phantom, using four microscope plates (blue), and pressing the sample in between them. b) The silicone mold used for the fabrication of the phantoms.*

This creates a very thin layer of the phantom, which can be optically characterized using the collimated transmission setup discussed in *Chapter Collimated Transmission*. For all the phantoms, three thin layers are created; one with only scattering agents, one with only absorption agents and one with both scattering and absorbing agents.

The mold is then placed into the vacuum chamber for a final degassing in the same way as described above. Once all remaining air bubbles are eliminated, the epoxy is left to cure in an oven set to 70 °C for a minimum duration of 30 minutes. After this, the phantom is solid enough to safely demold. See Figure 6 for a visualization of this fabrication process.

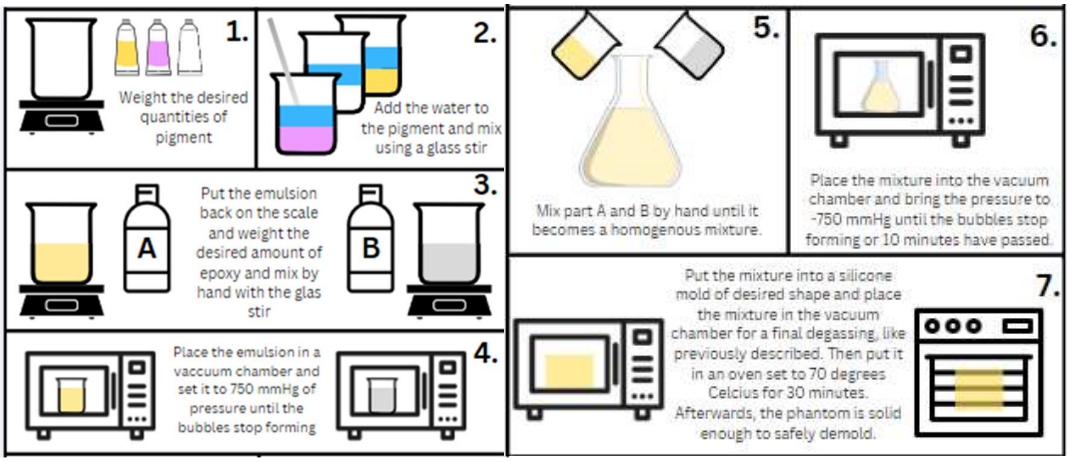

Figure 6*: Visualization of the fabrication method of the phantom.*

4.1.3 Single pigmented solid phantoms for validation purposes

Before fabricating the actual phantoms, the estimated optical properties of the pigments are validated. The phantoms for validation purposes exist of a single pigment mixed with epoxy, and are fabricated using the protocol described in *Section Phantom Fabrication*. The reduced scattering coefficient and absorption coefficient of the phantoms were estimated using the study from Walter and Jansen, which are displayed in Table 4.[15] However, even though the pigments were from the same manufacturer, the exact optical properties may vary per tube of paint. The exact concentrations of the single pigmented phantoms for validation purposes can be found in *Appendix A: Exact concentration of the single pigmented phantoms*.

Table 4: *The predicted absorption coefficient and reduced scattering coefficient normalized to the mass fraction included in epoxy resin for different pigments.*[15]

Pigment	Absorption coefficient per mg of pigment per gram of matrix material ($mm^{-1}/(mg/g)$)		Reduced scattering coefficient per mg of pigment per gram of matrix material ($mm^{-1}/(mg/g)$)	
	450 nm	*550 nm*	*450 nm*	*550 nm*
PY65	0.461	0	0.029	0.025
PY74	0.539	0	0.038	0.032
PR122	0.071	0.408	0.042	0.032
PR170	0.170	0.333	0.025	0.021
PW6	0.003	0.003	0.467	0.424

In addition to the phantoms fabricated with epoxy for validation purposes, the optical properties of the pigments are also evaluated in aqueous solutions by diluting the paint in water. These spectra can be found in *Appendix B: Measured attenuation spectra of pigments dissolved in water.*

After characterizing and validating the optical properties of the pigments in epoxy, the results are compared to Figure 4. The pigments are evaluated on their absorption and scattering properties around 450 nm and 550 nm, their stability to light exposure, the resemblance of the spectra to the study of Walter and Jansen and the ability to create a homogeneous phantom, ensuring minimal variance between different measurements.

4.1.4 Phantoms for TcB evaluation

Our phantom is designed to approximate the average optical properties of jaundiced neonatal skin at the sternum and forehead. Six different phantoms with different bilirubin concentrations were fabricated to mimic different states of jaundice:

- A phantom mimicking a bilirubin concentration of 0 µmol/L functioning as a control group (Table 5; phantom 1)
- A phantom mimicking a bilirubin concentration of 140 µmol/L, representing the standard phantom in Van Erk et at. (2019)[12] (Table 5; phantom 2)
- Two phantoms mimicking a bilirubin concentration of 150 µmol/L with a different amount of scattering, representing a healthy neonate (> 35 wks) at a postnatal age of 120 hours (Table 5; phantom 3 and 6)
- A phantom mimicking a bilirubin concentration of 200 µmol/L, considering that 200 µmol/L is a threshold for which a newborn (>35 wks) needs phototherapy to prevent brain injury at a postnatal age of 120 hours (Table 5; phantom 4)
- A phantom mimicking a bilirubin concentration of 250 µmol/L, representing a neonate with jaundice further above this threshold.[3,19,20] (Table 5; phantom 5)

This threshold for which a neonate needs phototherapy to prevent brain injury is based on the guideline provided for pediatricians and is valid for children born term (>35 weeks) with an additional risk factor. [8]

Using these concentrations, the desired quantities of yellow, magenta and titanium white can be calculated, using the data in Table 4 and the results from the validation experiment.

Table 5: *Calculated quantities of pigment for six phantoms and the mimicked absorption coefficient, scattering coefficient and TcB value.*

Phantom	Amount of pigment added (mg/g)	Mimicked absorption coefficient (mm^{-1})		Mimicked reduced scattering coefficient (mm^{-1})		Mimicked TcB value (µmol/L)
		450 nm	*550 nm*	*450 nm*	*550 nm*	
Composition phantom 1						
PY74	0.94	0.5	0.32	2.0	1.63	0
PR122	0.74					
PW6	4.28					
Composition phantom 2						
PY74	3.77	1.64	0.35	2.0	1.63	140
PR122	0.74					
PW6	4.28					
Composition phantom 3						
PY74	4.0	1.84	0.33	2.0	1.63	150
PR122	0.74					
PW6	4.28					
Composition phantom 4						
PY74	6.82	2.73	0.34	2.6	2.12	200
PR122	0.74					
PW6	5.56					
Composition phantom 5						
PY74	10.07	4.49	0.35	2.6	2.12	250
PR122	0.74					
PW6	5.56					
Composition phantom 6						
PY74	4.0	1.84	0.33	2.6	2.12	150
PR122	0.74					
PW6	5.56					

4.2 PHANTOM CHARACTERIZATION

4.2.1 Collimated Transmission

A collimated transmission (CT) setup was used for validation of the absorption and scattering coefficients of the phantoms. The CT setup measures attenuation spectra of the phantom layers in the 400-950 nm wavelength range. The light source in the setup is a halogen light source (AvaLight-HAL-S-Mini, Avantes, The Netherlands) and is directed through a 600µm core optical fiber (FC-UVIR600-1-BX,

Avantes, The Netherlands). The light first passes through a blue glass filter which attenuates the intensity in the higher wavelength range, resulting in a more uniform output across the visible light spectrum. The filtered light is then collimated by two lenses with a focal length of 25.4 mm (LA1951-A plano-convex Thorlabs, USA) and guided through a 4.5 mm aperture (SM1D12, Thorlabs, USA), illuminating the phantom. After the light is transmitted through the phantom, it is guided through two 4.5 mm apertures that are 32 cm apart from each other. The apertures are used to detect only the non-scattered light. Finally, the light is coupled into a 400 µm core fiber (FT400EMT, Thorlabs, USA), directing the light to the detecting spectrograph (AvaSpec-ULS2048CL-EVO-RS). This setup is visualized in Figure 7.

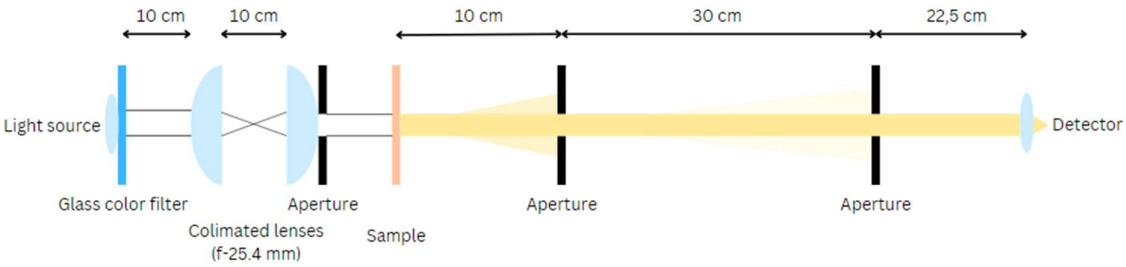

***Figure 7**: Collimated transmission setup to measure the optical properties of the fabricated phantoms.*

The collimated transmittance can be defined as:

$$T_C = \frac{\left(\frac{I_T(\lambda)}{\tau_T} - \frac{I_{B,T}(\lambda)}{\tau_{B,T}}\right)}{\left(\frac{I_0(\lambda)}{\tau_0} - \frac{I_{B,0}(\lambda)}{\tau_{B,0}}\right)} \quad (1)$$

with $I_T(\lambda)$ the transmitted spectrum through the phantom, $I_0(\lambda)$ the reference spectrum and $I_{B,T}(\lambda)$ and $I_{B,0}(\lambda)$ the background spectra for the sample and reference measurement, respectively. For the reference spectrum, measurements are done on a thin layer phantom consisting of only epoxy. All the measurements are normalized to the integration time of the measurement, τ.

Following the Lambert-Beer Law:

$$I\,(\lambda) = I_0(\lambda) \cdot e^{-\mu_t(\lambda)\cdot d} \quad (2)$$

with thickness (d) and total attenuation coefficient (μ_t), the collimated transmittance can be described as:

$$T_c(\lambda) = \frac{I(\lambda)}{I_0(\lambda)} = e^{-\mu_t(\lambda)\cdot d} \quad (3)$$

Rewriting formula 3 gives:

$$\mu_t(\lambda) = \frac{-\ln(T_c(\lambda))}{d} \quad (4)$$

The attenuation coefficient spectrum is composed of the sum of the absorption $\mu_a(\lambda)$ and the scattering coefficient $\mu_s(\lambda)$ spectra of the phantoms, as described in formula 5.

$$\mu_t(\lambda) = \mu_s(\lambda) + \mu_a(\lambda) \tag{5}$$

To easily distinguish between the scattering coefficient and absorption coefficient contribution to the spectra, every phantom is fabricated three times; one with only the scattering agent, one with only the absorption agent and one with the same quantities of both. With the use of formula 5, the absorption coefficient can then be calculated. The calculated composition of the phantoms for TcB-meter evaluation and their mimicked optical properties can be found in Table 4. The measured composition and concentration of the phantoms can be found in *Appendix E: Composition of the fabricated phantoms.*

The actual mimicked TcB value can be estimated using the measured absorption coefficient of the phantoms and formula 6, following from Table 1.

$$TcB_{value} = \frac{ln\left(\frac{\mu_a}{0,5}\right)}{0,0085} \tag{6}$$

4.2.2 Optical coherence tomography

To accurately calculate the absorption and scattering coefficient using Lambert-Beer, it is important to precisely know the thickness of the phantoms. An optical coherence tomography (OCT) system (ThorLabs Spectral Domain OCT Imaging System, 930 nm, 29 kHz) was used to characterize the thickness of the thin-layer phantoms. This setup is shown in Figure 8a.

An OCT A-scan is a representation of the sample reflectivity as a function of depth. In this study, the intensity peaks on the individual A-scans were fit to Gaussian functions. The distance between these peaks represents the optical pathlength and, when corrected with the refractive index, are used to determine the thickness of the phantom. Because the refractive index of the phantom is unknown, the thickness is measured between the microscope slide spacers where no pigment is present (Figure 5). The distance of the peaks is then corrected to the refractive index of air (n=1,003) to get the thickness of the phantom.[21] The thickness is measured at four different locations without pigment between the spacers and then averaged, as displayed in Figure 8b.

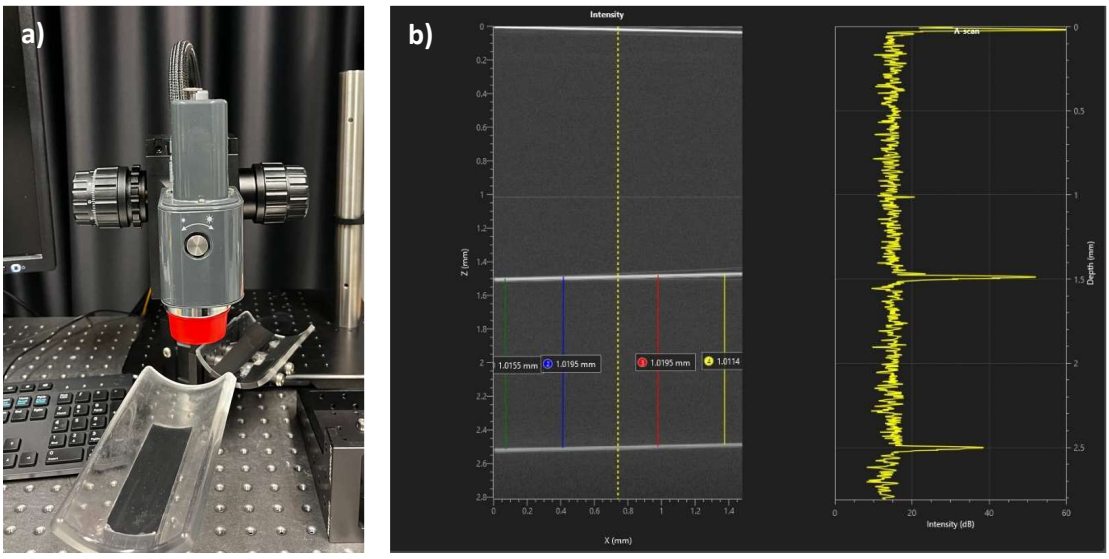

Figure 8: *a) The ThorImage OCT setup. b) An OCT scan to determine the thickness of the phantom, with a B-scan on the left side, with X-position on the X-axis and depth on the Y-axis. The four colored lines represent the four measurements. The yellow dotted line represents the location of the A-scan, which is shown on the right side, with Intensity (dB) on the X-axis and Depth (mm) on the Y-axis.*

4.2.3 Transcutaneous bilirubinometry

After measuring the optical properties of the phantom with Collimated Transmission, the phantoms are tested with a transcutaneous bilirubin meter. All TcB measurements are performed with the JM-105 (serial number B3601012, Dräger Medical, Lübeck, Germany). To optimize the measurement protocol and test the effect of different measurement conditions, the phantoms are measured in four different ways:

1. By measuring on the frontal surface of phantom, placing the TcB-meter straight onto the phantom.
2. By covering the measurement tip with a transparent layer of stretched Tegaderm™, similar to the approach of Dam-Vervloet et al..[13] The Tegaderm layer has a thickness comparable to the neonatal epidermal thickness.[12]
3. By covering the measurement tip with a transparent layer of stretched Tegaderm™ and the phantom with a layer of ultrasound gel, functioning as a refractive index coupling medium to replace the air between the measurement tip and the phantom.
4. By measuring on the back side of the phantom with a transparent layer of stretched Tegaderm™ without ultrasound gel, to test the influence of different surfaces.

For all the phantoms, the TcB was measured as the average +/- standard deviation (SD) of five measurements at five different locations for a good estimate of the variation in the data, similar to the approach of Dam-Vervloet et al. (2024). [13] The locations per phantom can be found in *10.4 Appendix D: Measured attenuation spectra of the individual pigments.*

5 RESULTS

5.1 VALIDATION OF PIGMENTS IN SINGLE PIGMENTED SOLID PHANTOMS

The measured attenuation spectra for the yellow and magenta pigments mixed with epoxy are shown in Figure 9a and 9c, averaging measurements at five different locations in the sample. Figure 9b and 9d display the spatial variance between the different measurement locations, informing us about the homogeneity of the pigment distribution. The individual spectra per pigment with standard deviation can be found in *Appendix D: Measured attenuation spectra of the individual* pigments.

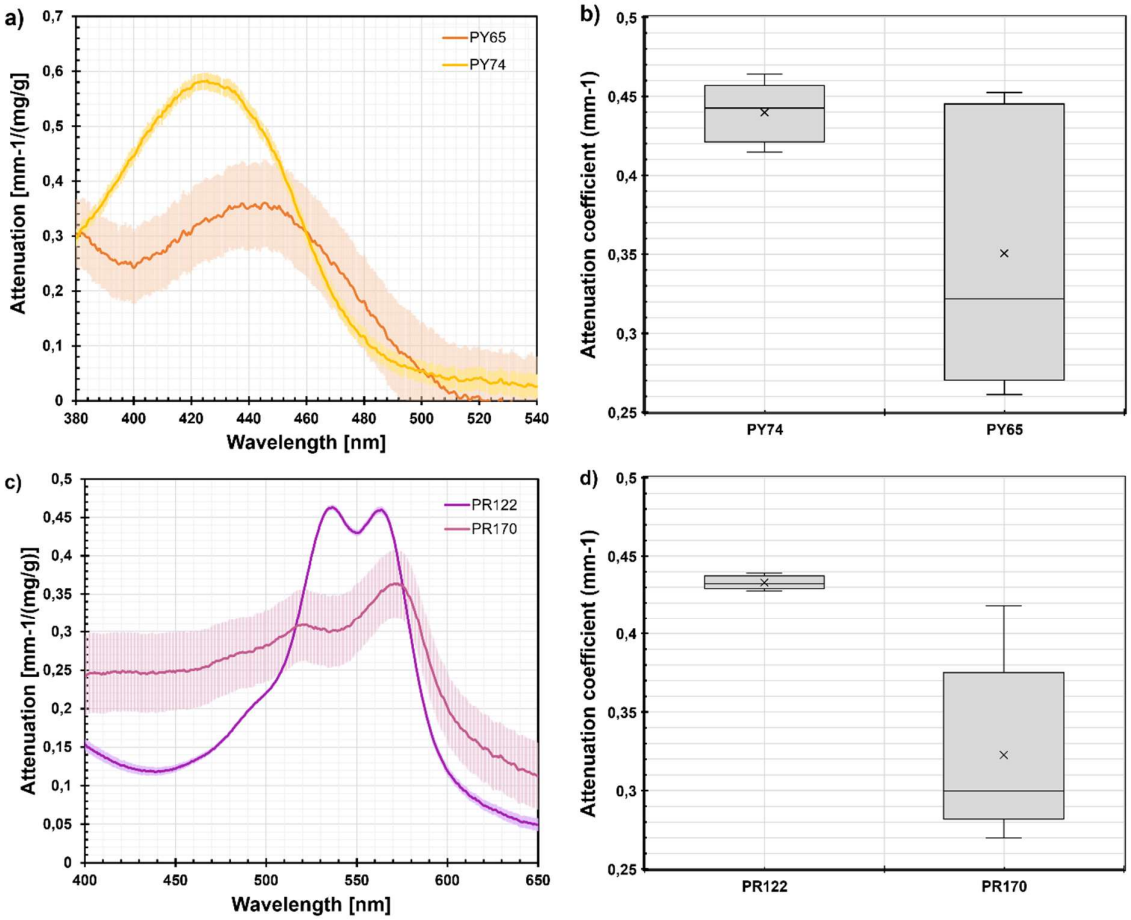

Figure 9 *a) The averaged attenuation spectra over five measurements of the yellow pigments in single pigmented solid phantoms normalized to the mass factor (milligram of pigment per gram of epoxy). b) The spatial variance between the different measurement locations of the same single pigmented solid phantom for the yellow pigments at 450 nm. The boxes represent the first and third quartiles, the line represents the median and the cross represents the average value. The whiskers end at the minimum and maximum value of the measurements. c) The averaged attenuation spectra over five measurements of the magenta pigments in single pigmented solid phantoms normalized to the mass factor (milligram of pigment per gram of epoxy). d) The spatial variance between the different measurement locations of the same single pigmented solid phantom for the magenta pigments at 550 nm. Also here, the boxes represent the first and third quartiles, the line represents the median and the cross represents the average value. The whiskers end at the minimum and maximum value of the measurements.*

For the scattering pigments, a series of single pigmented phantoms was fabricated. Figure 10a shows the averaged attenuation spectra of 8 phantoms with different concentrations of scattering agent (PW6), measured at three different locations, three measurements per location. Figure 10b shows the averaged measured attenuation versus concentration.

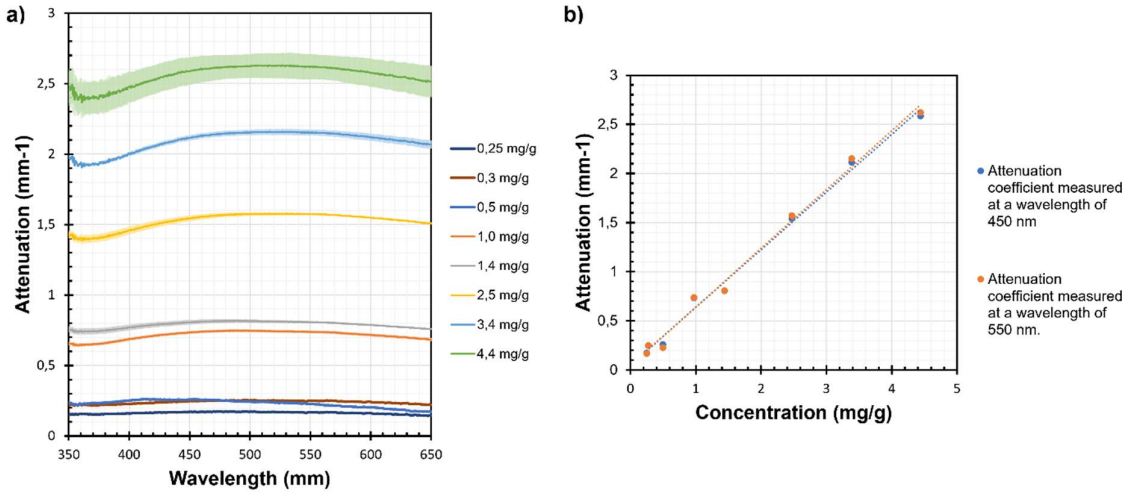

Figure 10 *a) The averaged attenuation spectra of different concentrations of titanium white (PW6) in single pigmented phantoms with standard deviation. b) The attenuation of the series single pigmented phantoms with white pigment (PW6) against the concentration of these phantoms, showing a linear correlation between attenuation and concentration for 450 nm (blue) and 550 nm (orange).*

5.2 PHANTOMS FOR TCB EVALUATION

The phantoms made for the evaluation of TcB meters were measured with the collimated transmission setup and a TcB meter (Dräger JM-105). Additionally, the phantoms were viewed under a microscope, evaluating the homogeneity of the surface.

5.2.1 Collimated Transmission measurements

In total, six phantoms were fabricated following Table 5. The exact composition per phantom and its concentration can be found in *Appendix E: Composition of the fabricated phantoms*. For all six phantoms, three thin layers were fabricated, as displayed in Figure 11.

Here, the assumption was made that the attenuation coefficient measured in the scattering layer is caused only by scattering and therefore equal to the scattering coefficient ($\mu_t \approx \mu_s$) and the attenuation coefficient measured in the absorption layer is caused only by absorption and therefore equal to the absorption coefficient ($\mu_t = \mu_a$). In that way, the attenuation from the phantom layer is a sum of the separately measured μ_s and μ_a, such that $\mu_t \approx \mu_s + \mu_a$.

Figure 11 *The three fabricated phantom layers of phantom 5, with P5 the phantom layer, S5 the layer with only scattering agent of and A5 the layer with only the absorbing pigments.*

Table 6 presents an overview of the actual mimicked TcB values per phantom based on the absorption coefficients and the data from Table 1. The actual mimicked TcB value in Table 6 is based on formula 6 in *4.2.2 Optical coherence tomography* and the measured absorption coefficient in the absorption layer. The variation of mimicked TcB value from Table 5, may stem from pigment that failed to dissolve during fabrication.

Table 6: *Overview of attenuation coefficients at 450 and 550 nm, and mimicked TcB values of six phantoms fabricated in this study.*

Phantom	Wavelength	Attenuation coefficient of absorption agent only ($\mu_t \approx \mu_a$) (mm^{-1})	Actual mimicked TcB value based on the measured absorption coefficient (µmol/L)
1	450 nm	0,61	0
	550 nm	0,45	
2	450 nm	1,43	102
	550 nm	0,65	
3	450 nm	1,40	127
	550 nm	0,63	
4	450 nm	2,11	177
	550 nm	0,90	
5	450 nm	2,91	208
	550 nm	1,12	
6	450 nm	1,50	142
	550 nm	0,75	

The optical properties of every thin layer are measured with the Collimated Transmission setup at three different locations in the sample, five measurements at each location. This creates an average of 15 measurements. The spectra of all phantoms are displayed in Figure 12.

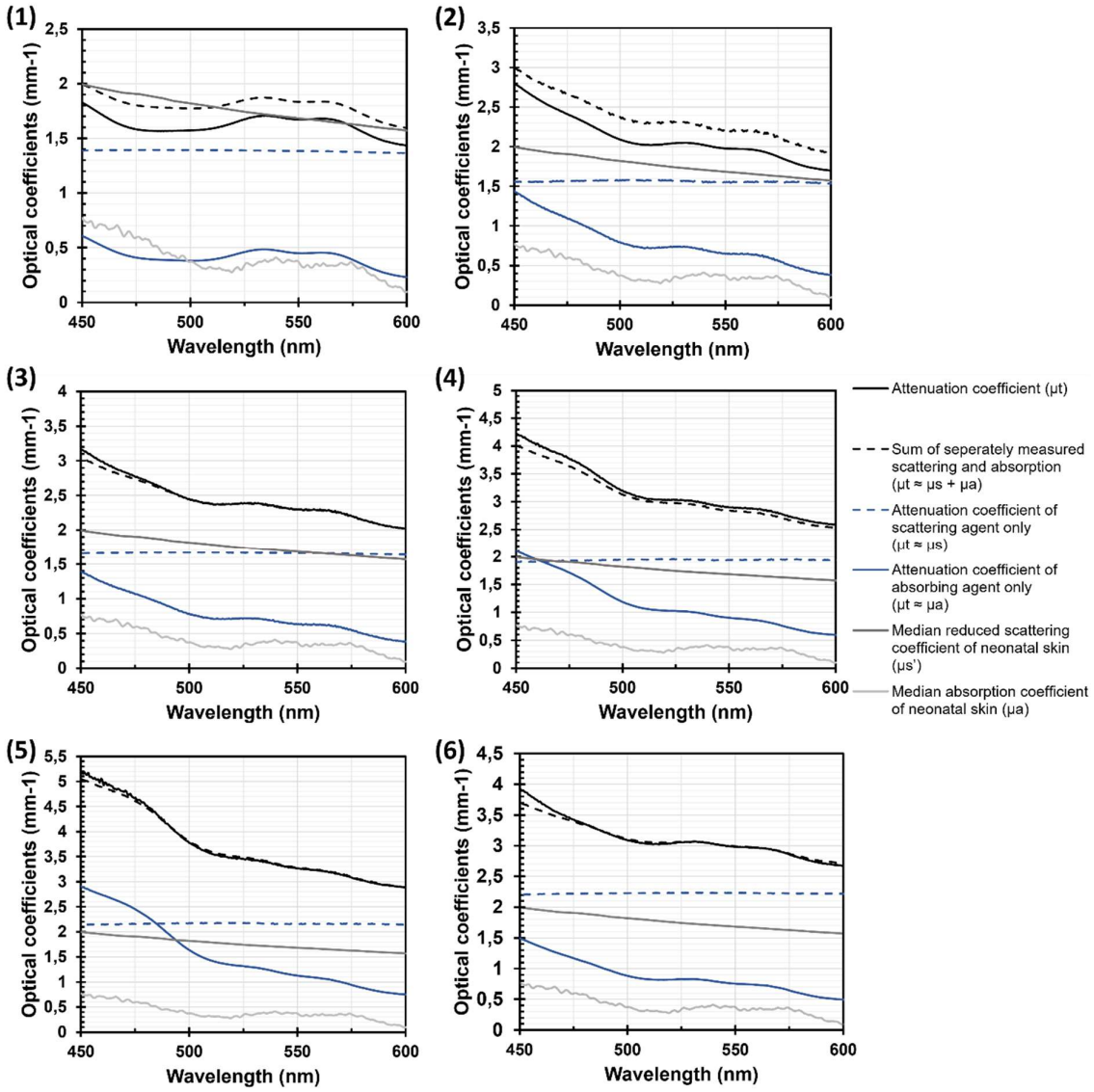

Figure 12: *The spectra of all six fabricated phantoms (1-6) including the median reduced scattering coefficient (μ_s') and absorption coefficient (μ_a) of neonatal skin as studied by Bosschaart et al.*[7]

5.2.2 TcB-meter measurements

The TcB-meter measurements were done with the Dräger JM-105 using different measuring protocols. The complete datasets can be found in *Appendix F: TcB datasets for the Phantoms.*

5.2.2.1 TcB measurements using a Tegaderm film

All phantoms were measured by covering the measurement tip with a stretched Tegaderm film. The TcB meter was placed on the phantom with an angle of 90°, ensuring that light getting away from the sides remains to a minimum. Every phantom was measured on five different locations, ten data points per location leading to a total of 50 measurements per phantom. The results of these measurements are displayed in Figure 13.

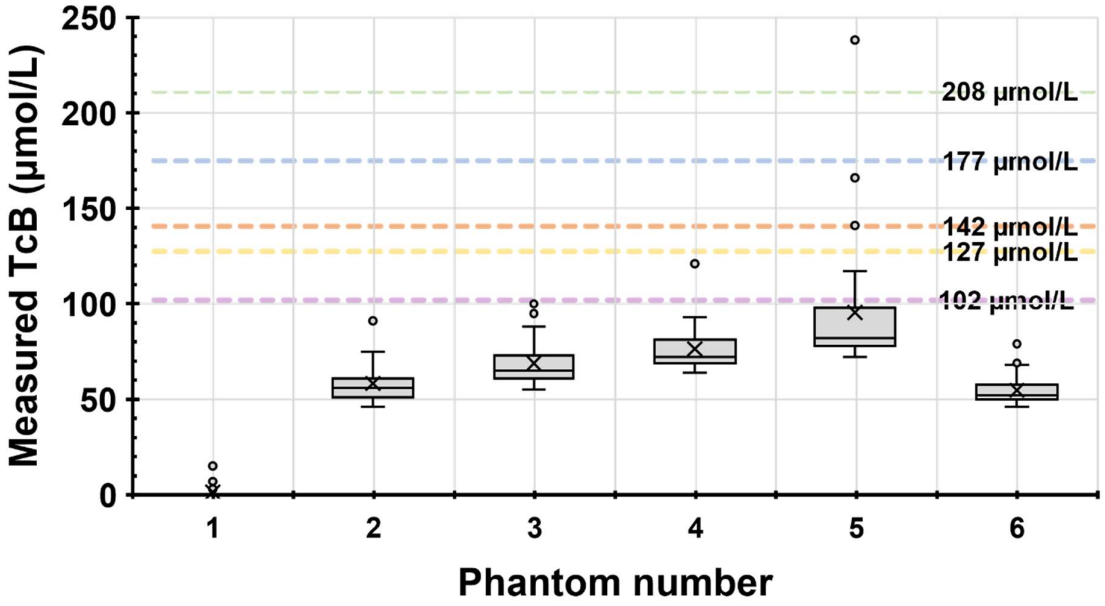

***Figure 13**: A boxplot presenting a comparison of the TcB measurements on phantom 1,2, 3, 4, 5 and 6 mimicking a bilirubin concentration of 0, 102, 127, 177, 208 and 142 µmol/L, respectively. The measurements were done while using a Tegaderm film on the measuring tip. The boxes represent the first and third quartiles, the line represents the median and the cross represents the average value. The whiskers end at the minimum and maximum value of the measurements. The dots represent the outliers of the dataset.*

Measurements on Phantom 2 were done twice with this same protocol. The difference between the measurements was the angle between the TcB-meter and the phantom. The measurements in the second data set were all assured of a 90° angle between the meter and the phantom, while this was not the case in the first data set. The first data set shows an average of 106,3 µmol/L over 50 measurements with a standard deviation of 57,9 µmol/L, while the second data set shows an average of 58,2 µmol/L over 25 measurements with a standard deviation of 10,0 µmol/L, as shown in Figure 14.

The control group phantom, mimicking a concentration of 0 µmol/L, shows an average measured TcB of 1,40 µmol/L over 50 measurements with a standard deviation of 3,1 µmol/L.

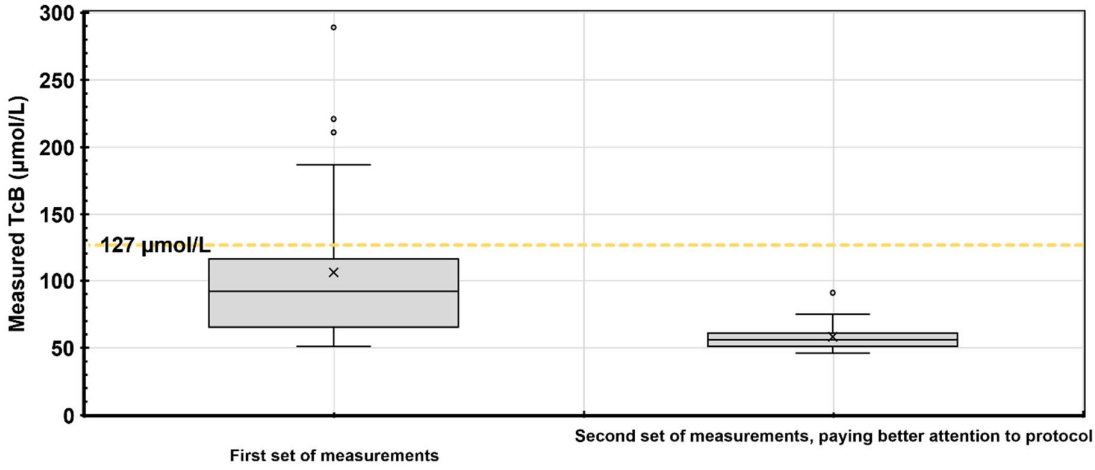

Figure 14: *A boxplot comparing two sets of measurements done on the same phantom at the same locations, with the same protocol. The second set of measurements was done with an improved measurement protocol. The boxes represent the first and third quartiles, the line represents the median and the cross represents the average value. The whiskers end at the minimum and maximum value of the measurements.*

5.2.2.2 TcB measurements with ultrasound gel

On Phantom 2, 5 and 6, measurements were done with ultrasound gel covering the surface of the phantoms and using a Tegaderm film to protect the TcB-meter from damaging. This showed a significant increase in the measured TcB, suggesting that the air between the measuring tip and the phantom causes an unreliable measurement of the phantoms. The difference in average TcB and standard deviation are shown in Table 7.

Table 7: *Average TcB measurements on Phantoms 2, 5 and 6 without and with ultrasound gel. Phantom 2, 5 and 6 mimics a bilirubin concentration of 102, 208 and 142 µmol/L, respectively.*

Phantom	Average TcB when measuring without ultrasound gel (µmol/L) with standard deviation (µmol/L)	Average TcB when measuring with ultrasound gel (µmol/L) with standard deviation (µmol/L)
2	58,2 ± 10,0	116,0 ± 29,1
5	95,4 ± 168,1	35,6 ± 61,2
6	54,7 ± 7,4	155,2 ± 18,7

5.2.2.3 TcB measurements on Phantom 6 using different protocols

Four different measurement protocols are used on Phantom 6. The results are displayed in Figure 15. According to calculations from the Collimated Transmission measurements, Phantom 6 mimics a TcB value within the range of 125 and 142 µmol/L. The average measured TcB obtained from Phantom 6, was 73 µmol/L without Tegaderm, 55 µmol/L with Tegaderm and 155 µmol/L with ultrasound gel and Tegaderm. The standard deviation calculated for these measurements are 9,8 µmol/L, 7,39 µmol/L and 18,7 µmol/L respectively. The backside of the phantom is more reflective than the front, leading to

more reflected light and lower TcB measurements. The average TcB measured on the backside of the phantom is 44,5 µmol/L with a standard deviation of 4,9 µmol/L.

Figure 15: *Measurements on Phantom 6, which should mimic a TcB value ranging from 125 µmol/L to 140 µmol/L, using four different measuring protocols. The boxes represent the first and third quartiles, the line represents the median and the cross represents the average value. The whiskers end at the minimum and maximum value of the measurements.*

To evaluate the spatial variance of the phantom, measurements are done in five different locations, five measurements in each location. The spatial variance of the measurements without Tegaderm, with Tegaderm and with ultrasound gel and Tegaderm are shown in Figure 16.

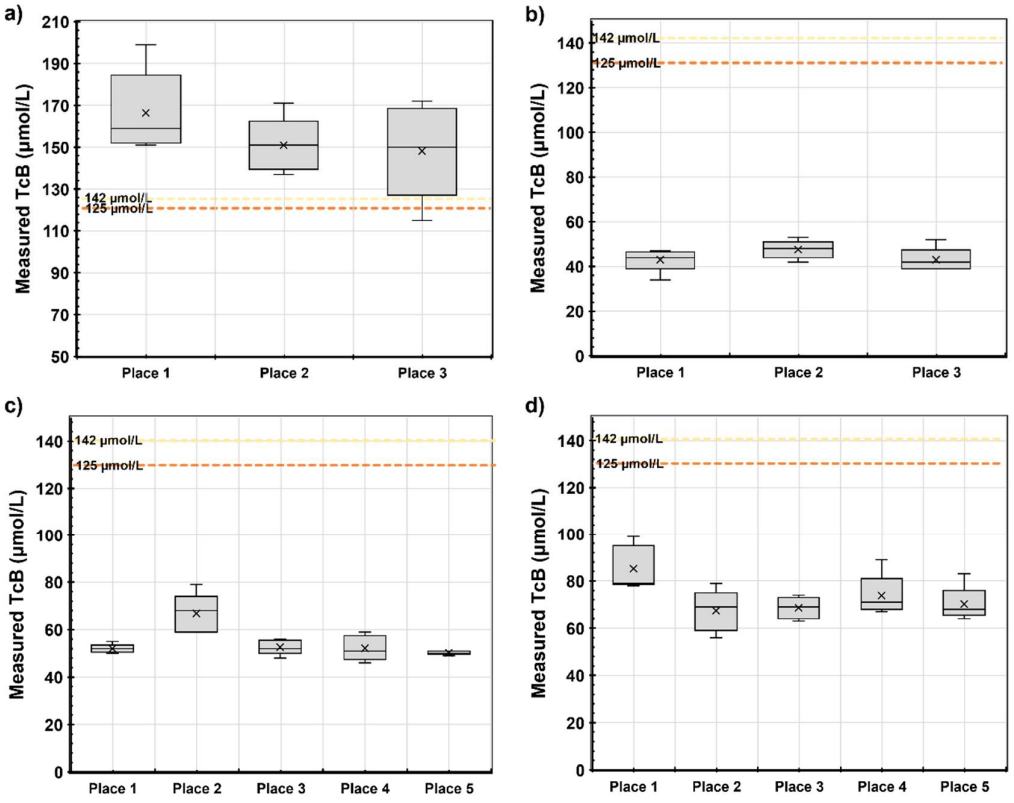

Figure 16: *The spatial variance between the different measurement locations of Phantom 6, measured with ultrasound and Tegaderm (a), on the other side of the phantom (b), with Tegaderm (c) and without Tegaderm (d). The boxes represent the first and third quartiles, the line represents the median and the cross represents the average value. The whiskers end at the minimum and maximum value of the measurements.*

6 DISCUSSION

The main purpose of this thesis was to fabricate and characterize an optically stable phantom for evaluating TcB-meters. Hereto, the different pigments were first characterized using Collimated Transmission and compared to the findings of Walter and Jansen.[15] The spectra in *Appendix D: Measured attenuation spectra of the individual pigments* show similar behavior to the earlier results from Walter and Jansen.[15] However, they do not exactly match, which can be due to the fact that they were from a different batch of fabricated paint, suggesting that different tubes of paint from the same manufacturer can still exhibit different optical properties. The epoxy used could also play a role, since the exact optical properties of epoxy might also vary per batch. Another reason that might have caused this deviation in results could be the method to optically characterize the phantoms. While Duco and Jansen use Inverse Adding Doubling, this study uses collimated transmission and the separation of the phantom in absorbing agents only and scattering agents only to distinguish the absorption coefficient and the scattering coefficient in the attenuation spectra.

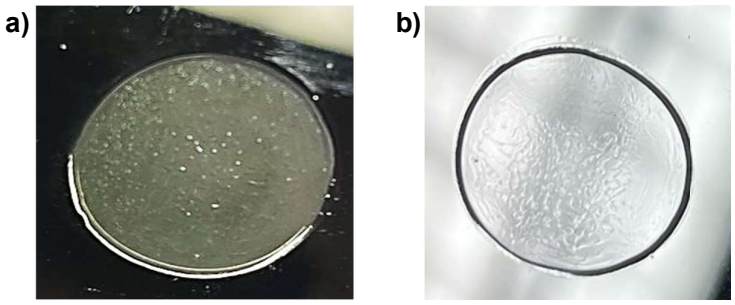

***Figure 17**: A thin layer phantom with pigment PW6 and epoxy, showing a) several air bubbles throughout the phantom and b) an atypical structure within the phantom.*

In addition to the results deviating from literature, pigments PY65 and PR170 also show a larger standard deviation than PY74 and PR122, as shown in **Figure 23** and **Figure 24** in *Appendix D: Measured attenuation spectra of the individual pigments.* This indicates a variability within the phantom, potentially impacting the reliability of future phantoms for TcB-meter evaluation. This variability, highlighted by the spatial variance in Figure 9b and d, raises questions about the homogeneity of the phantoms and might be caused by the efficiency with which the pigments are mixed into epoxy. Another cause for this could be the influence of air bubbles within the thin layer of the single pigmented phantoms, as seen in Figure 17a.

For the collimated transmission, a reference phantom is used to calculate the transmission and attenuation. However, the introduction of air bubbles in the thin layer of the reference phantom creates possible higher variation within the attenuation spectra at certain parts. Additionally, the epoxy creates an atypical structure within the single pigmented phantoms as shown in Figure 17b.

Comparing the spectra of the white pigments to literature, they do not match their profile. There is no decline visible in the measured wavelength range and the scattering coefficient seems lower. This is not accurately comparable, since the reduced scattering coefficient (μ_s'), as presented in data from Duco and Jansen, is a different parameter compared to the scattering coefficient (μ_s). The anisotropy of the epoxy and pigments have not been studied, making it difficult to calculate the reduced scattering coefficient from the results of this study. However, the white pigment consists of titanium dioxide, for which the anisotropy has been reviewed, as displayed in Figure 18.

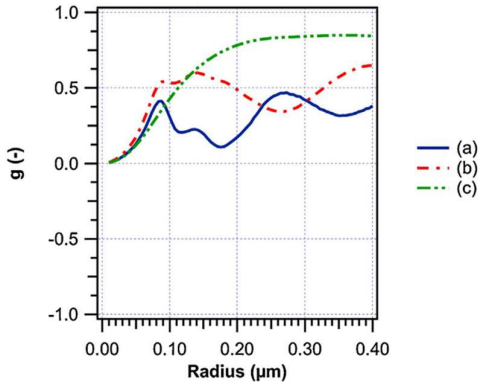

Figure 18: *The wavelength-average anisotropic factor of a) TiO2 in air, b) TiO2 in polymer matrix, c) air-bubble in polymer matrix against particle size. Figure adapted from Ager and McLoughlin (2014)*[22]

The average particle size of common used commercial titanium dioxide generally has a particle size ranging from 200 nm to 300 nm.[23] As seen in Figure 18, TiO_2 in a polymer matrix has a anisotropic factor of 0,27 for a radius of 0,25 µm. Therefore, $\mu_s'=0{,}73\mu_s$ using the formula introduced in *Section Optical properties of neonatal skin.* As shown in Figure 3, the neonatal skin shows a spread of reduced scattering, with a median μ_s' of 1,8 mm^{-1} at 450 nm. Phantom six exhibited the highest scattering coefficient of 2,2 mm^{-1}, equivalent to a reduced scattering coefficient of 1,61 mm^{-1}. Studies have shown that the reduced scattering coefficient affects the results of TcB-readings, suggesting that this could be a reason for inaccuracies in TcB-measurements.[12]

The series of white pigmented phantoms do show the same spectrum for different concentrations, only varying in magnitude of attenuation, as shown in Figure 10b.

6.1 Variability and stability of fabricated phantoms for TcB measurements

The variability and stability of the fabricated phantoms are a crucial aspect in the development of a reliable and optically stable phantom for TcB measurements. These factors directly impact the phantom's ability to accurately mimic a TcB concentration for effective calibration and validation purposes. Variability of the phantoms can be caused by several factors, including inconsistencies in the

mixing of the pigments with the Epoxy, variations in curing conditions, and the presence of air bubbles, as previously mentioned.

At the surface of some of the phantoms show mostly white flakes of pigment, which are not well integrated within the epoxy, as displayed in Figure 19, possibly being another cause for the variability of the TcB measurements. Twice as much the water was added in Phantoms 4-6 to the PW6-pigment, as an attempt to enhance the integration of the pigments in the phantom more homogeneously, which turned out successful. On the surface of phantom 4, 5 and 6, a smaller number of white flakes of pigment are visible in comparison to phantom 1, 2 and 3, suggesting that adding more water to the white pigments is a successful alteration to the fabrication process.

Figure 19: *The six fabricated phantoms (phantom 1 on top left, phantom 6 on bottom right, from left to right), showing some irregularities on the surface in the form of white or red flakes caused by pigments not thoroughly mixed into the epoxy.*

Furthermore, the stability of the fabricated phantoms over time is an important aspect to ensure consistent readings for the calibration of the TcB meter. Exposure to light, temperature fluctuations, and physical handling can all affect the stability. However, due to the limited time available for this research, the stability of the phantoms could not be studied. Section *Outlook* provides a plan to test this stability.

6.2 OPTIMIZATION OF THE MEASURING PROTOCOL

In this thesis, different protocols were used for the measurements with the TcB-meter. The use of Tegaderm film resulted in lower TcB readings, with an average standard deviation of 13,5 µmol/L. This can be caused by scattering of the Tegaderm films or possible air bubbles under the Tegaderm film, possibly invisible to the eye. The maximum range of TcB readouts within a data set is 57 µmol/L, which is higher than the given spread of 40 µmol/L by Dräger. This suggests that the measuring protocol needs improvement by better coverage of the measurement tip with Tegaderm or the use of different films. This variance while using Tegaderm film is however in line with literature. It would be preferable not to use the Tegaderm, as the phantom causes no damage to the TcB-meter and Tegaderm can influence the measurements.

Measurements on the backside of the phantom result in even lower TcB-measurements. The backside of the phantom appears more reflective, which could cause the lower readouts, as higher reflectivity can cause more light to bounce off the surface instead of penetrating it, reducing the amount of light absorbed and subsequently detected by the TcB-meter.

Furthermore, the epoxy exhibits a solid rock-hard surface, while the skin has a much more flexible and soft tissue, with the ability to dent. When pressing the TcB-meter on the skin, it lightly dents the skin, causing the entire measuring tip of the TcB-meter to directly be in contact the skin. The epoxy does not dent at all, resulting in air between (parts of) the measurement tip and the phantom. This causes an unreliable TcB measurement, much lower than the actual mimicked TcB, which is noticeable in the measured TcB of all phantoms when measuring without ultrasound gel.

With the use of ultrasound gel, TcB readouts resulted in values much closer to the mimicked TcB. This suggests that a gel with refractive index comparable to water can be applied on the surface of the phantom to enhance TcB measurements. However, the use of ultrasound gel also comes with a higher standard deviation, going from 7,4 µmol/L to 13,7 µmol/L, again indicating the necessity of improvement of the protocol. A reason for this higher standard deviation could be the presence of air bubbles in the ultrasound gel. The use of another gel or liquid solution with refractive index comparable to water could possibly reduce this.

Figure 14 indicates the importance of a measurement protocol, showing two sets of measurements done on the same phantom with significantly different results. The first set of measurements was done when I was still familiarizing myself with the technique, while the second set was done last, by which time my technique had significantly improved. Should the phantom be used for the calibration and evaluation of TcB-meters, it will be necessary to establish a straightforward protocol to ensure consistent readouts.

7 CONCLUSION

This study successfully developed a tissue phantom that mimics the neonatal skin's optical properties, which can potentially be used for the evaluation of transcutaneous bilirubin meters. The results confirm that the specific mix of epoxy resin and pigments (PR122, PY74 and PW6) can create a solid phantom, suitable for measurements with a TcB-meter. Future work should focus on minimizing the variability observed in the TcB measurements by improving the measuring protocol and evaluating long term stability of the phantoms.

8 OUTLOOK

Although the results of this study show great promise for the implementation of an optically stable phantom in the evaluation of the TcB-meter, it is important to further investigate several aspects in future research.

As previously mentioned in *Section Optimization of the measuring protocol*, the angle between the phantom and the TcB-meter causes variations in TcB readings. A possible solution to this is creating a hole in the phantom with the exact size of the measuring tip, or an additional layer with a hole in it on top of the phantom. This is visualized in Figure 20. By only measuring through the hole, the angle remains stable throughout different measurements and light cannot escape through the sides. Another option is to add a cylinder on the bottom of the silicone mold, creating a hole in the phantom during the fabrication process.

Figure 20: *Visualization of an additional TcB-measuring protocol that could be used to ensure reliable and consistent readouts.*

Additionally, the use of ultrasound gel can remove the air between the phantom and the measuring tip, ensuring direct contact. As shown in the results of this study, the use of ultrasound gel gave readings much closer to the mimicked TcB. Further use of ultrasound gel is thus recommended, and, as stated in section *6.2 Optimization of the measuring protocol,* another type of gel or liquid solution with refractive index comparable to water could be studied to reduce the impact of air bubbles present in ultrasound gel.

Furthermore, these phantoms mimic the total absorption and the optical scattering of neonatal skin, while earlier research revealed that skin color influences the TcB-readings.[13] The addition of a pigment layer mimicking melanin absorption in the epidermis could enhance the phantom even further and ensure more accurate TcB readings for different skin colors.

The aim for my thesis was to fabricate an optically stable phantom. Unfortunately, the limited time for this study made it impossible to test the phantoms on stability over a longer time. This stability could be tested by measuring the attenuation coefficient weekly with the collimated transmission setup, for the duration of 6 months. This should be done in the same manner as this study, by measuring at five different locations with five measurements at each location over the course of a year. Besides measurements with the collimated transmission, the phantom should also be evaluated on stability, by weekly measuring the TcB-value of the phantom with the TcB-meter and testing the results on variability.

Lastly, it is recommended to test the reproducibility of the phantom fabrication process. This could be done by creating different phantoms with identical pigment concentrations and evaluating them with the collimated transmission setup for variability in attenuation coefficient.

9 BIBLIOGRAPHY

1. Ansong-Assoku B, Shah SD, Adnan M, Ankola PA. Neonatal Jaundice. *Alzheimer's Dement Diagnosis, Assess Dis Monit*. 2023;13(3):1-4. Accessed March 6, 2024. https://www.ncbi.nlm.nih.gov/books/NBK532930/

2. Zhou Y, Zhang C, Yao DK, Wang L V. Photoacoustic microscopy of bilirubin in tissue phantoms. *J Biomed Opt*. 2012;17(12):126019. doi:10.1117/1.JBO.17.12.126019

3. Dam-Vervloet, A.J. ir (PhD). *Chapter 1-8 Proefschrift_Optimalization of the Detection and Therapy of Hyperbilirubinemia_V3*.; 2024.

4. Kemper AR, Newman TB, Slaughter JL, et al. Clinical Practice Guideline Revision: Management of Hyperbilirubinemia in the Newborn Infant 35 or More Weeks of Gestation. *Pediatrics*. 2022;150(3):2022058859. doi:10.1542/PEDS.2022-058859/188726

5. Bosschaart N, Kok JH, Newsum AM, et al. Limitations and opportunities of transcutaneous bilirubin measurements. *Pediatrics*. 2012;129(4):689-694. doi:10.1542/peds.2011-2586

6. Dani C, Hulzebos C V., Tiribelli C. Transcutaneous bilirubin measurements: useful, but also reproducible? *Pediatr Res 2020 894*. 2020;89(4):725-726. doi:10.1038/s41390-020-01242-3

7. Bosschaart N, Mentink R, Kok JH, van Leeuwen TG, Aalders MCG. Optical properties of neonatal skin measured in vivo as a function of age and skin pigmentation. *J Biomed Opt*. 2011;16(9):097003. doi:10.1117/1.3622629

8. Samenvattingskaart | Babyzietgeel. Accessed March 13, 2024. https://www.babyzietgeel.nl/kinderarts-samenvattingskaart

9. Richtlijn - NVK. Accessed March 7, 2024. https://www.nvk.nl/themas/kwaliteit/richtlijnen/richtlijn?componentid=258506752&tagtitles=Acute%252bKindergeneeskunde%2CHematologie%2CNeonatologie%2CSectie%252bIntensive%252bCare%252bKinderen%252b(SICK)%2CSectie%252bKinderhematologie%252b(SKH)%2CSectie%252bNeonatologie%252b(SN)

10. Engle WD, Jackson GL, Engle NG. Transcutaneous bilirubinometry. *Semin Perinatol*. 2014;38(7):438-451. doi:10.1053/J.SEMPERI.2014.08.007

11. Jonasson H, Fredriksson I, Carl SB, et al. In vivo characterization of light scattering properties of human skin in the 475- to 850-nm wavelength range in a Swedish cohort. *https://doi.org/101117/1JBO2312121608*. 2018;23(12):121608.

doi:10.1117/1.JBO.23.12.121608

12. van Erk MD, Dam-Vervloet AJ, de Boer FA, Boomsma MF, Straaten H van, Bosschaart N. How skin anatomy influences transcutaneous bilirubin determinations: an in vitro evaluation. *Pediatr Res 2019 864*. 2019;86(4):471-477. doi:10.1038/s41390-019-0471-z

13. Dam-Vervloet AJ, Morsink CF, Krommendijk ME, et al. Skin color influences transcutaneous bilirubin measurements: a systematic in vitro evaluation. *Pediatr Res 2024*. Published online February 17, 2024:1-5. doi:10.1038/s41390-024-03081-y

14. Lualdi M, Colombo A, Farina B, Tomatis S, Marchesini R. A phantom with tissue-like optical properties in the visible and near infrared for use in photomedicine. *Lasers Surg Med*. 2001;28(3):237-243. doi:10.1002/LSM.1044

15. Walter AB, Jansen ED. Development of a platform for broadband, spectra-fitted, tissue optical phantoms. *J Biomed Opt*. 2023;28(02):1-20. doi:10.1117/1.jbo.28.2.025001

16. Veenstra C, Petersen W, Vellekoop IM, Steenbergen W, Bosschaart N. Spatially confined quantification of bilirubin concentrations by spectroscopic visible-light optical coherence tomography. *Biomed Opt Express*. 2018;9(8):3581. doi:10.1364/BOE.9.003581

17. Ntombela L, Adeleye B, Chetty N. Low-cost fabrication of optical tissue phantoms for use in biomedical imaging. *Heliyon*. 2020;6(3):e03602. doi:10.1016/J.HELIYON.2020.E03602

18. Sieryi O, Popov AP, Kalchenko V, Bykov A V., Meglinski I. Tissue-mimicking phantoms for biomedical applications. 2020;(April):39. doi:10.1117/12.2560174

19. Chen YY, Tzeng SY, Lin YL, Chu KY, Tseng SH. Precisely discerning the bilirubin concentration of turbid samples using diffuse reflectance spectroscopy. *Opt InfoBase Conf Pap*. 2016;(January):3-5. doi:10.1364/FIO.2016.FW3C.3

20. Dräger Medical System I. Manual JM-105. instructions for Use. Published online 2016. Accessed March 7, 2024. https://www.draeger.com/Products/Content/jm-105-sw-120-ifu-9510905-en.pdf

21. Ciddor PE. Refractive index of air: new equations for the visible and near infrared. *Appl Opt Vol 35, Issue 9, pp 1566-1573*. 1996;35(9):1566-1573. doi:10.1364/AO.35.001566

22. Auger JC, McLoughlin D. Theoretical analysis of light scattering properties of encapsulated rutile titanium dioxide pigments in dependent light scattering regime. *Prog Org Coatings*. 2014;77(11):1619-1628. doi:10.1016/J.PORGCOAT.2014.05.005

23. Song J, Qin J, Qu J, et al. The effects of particle size distribution on the optical properties of titanium dioxide rutile pigments and their applications in cool non-white coatings. *Sol Energy Mater Sol Cells*. 2014;130:42-50. doi:10.1016/J.SOLMAT.2014.06.035

10 APPENDIX

10.1 APPENDIX A: EXACT CONCENTRATION OF THE SINGLE PIGMENTED PHANTOMS

Pigment		**PR122**	**PR170**	**PY65**	**PY74**	**PW6**	**PW6**	**PW6**	**PW6**	**PW6**	**PW6**	**PW6**
Concentration (mg/g)		1,21	0,981	0,231	0,368	0,25	0,495	0,974	1,44	2,47	3,39	4,44
Attenuation (mm^{-1})	*450 nm*	0,147	0,243	0,0819	0,161	0,172	0,258	0,734	0,806	1,54	2,11	2,59
	550 nm	0,519	0,312	0	0,011	0,247	0,227	0,738	0,807	1,57	2,15	2,62
Attenuation normalized to concentration (mm^{-1}/(mg/g))	*450 nm*	0,122	0,247	0,354	0,437	0,688	0,521	0,753	0,560	0,624	0,622	0,583
	550 nm	0,430	0,318	0	0,029	0,988	0,459	0,758	0,559	0,636	0,634	0,590

10.2 APPENDIX B: MEASURED ATTENUATION SPECTRA OF PIGMENTS DISSOLVED IN WATER

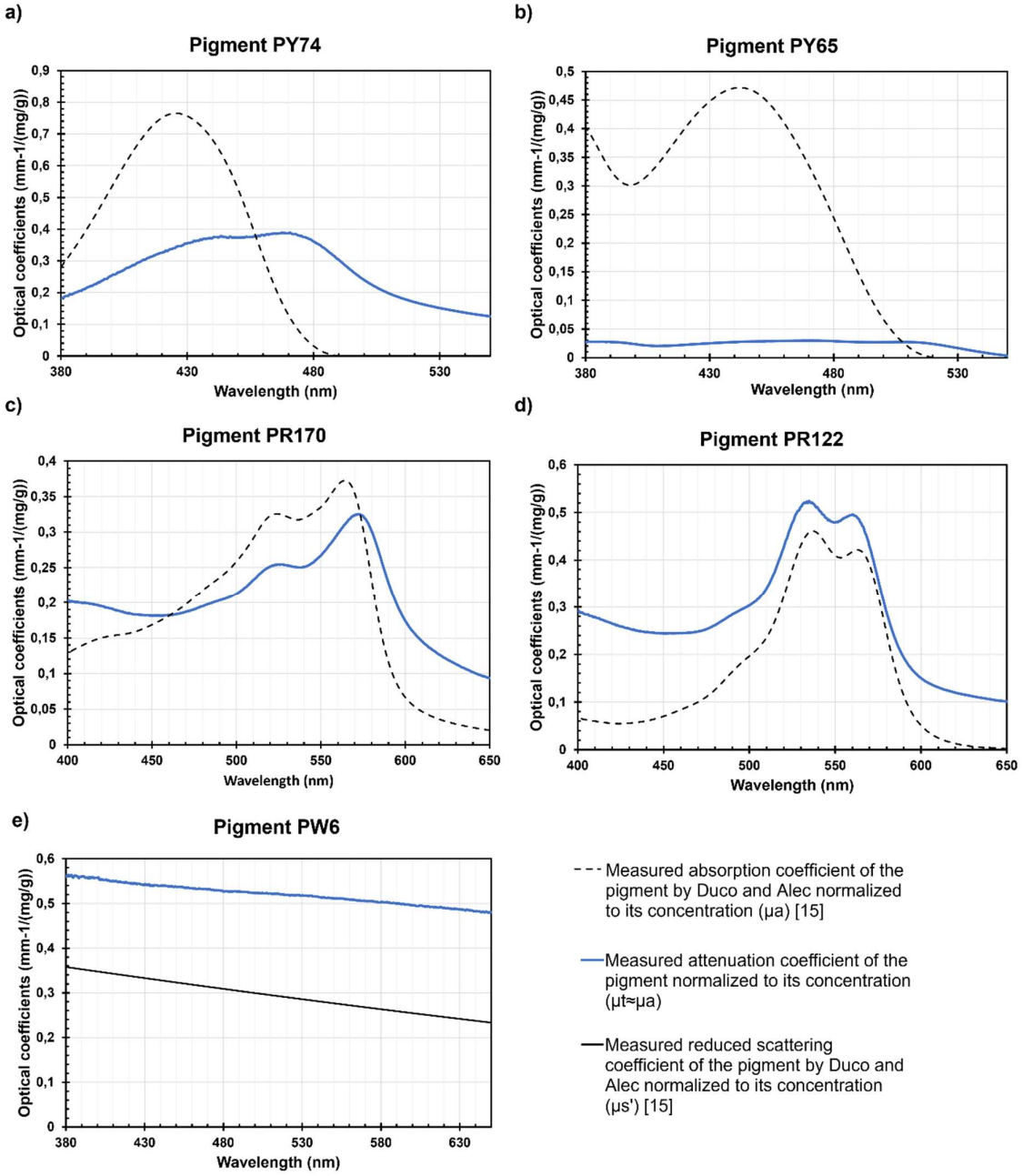

***Figure 21**: Averaged measured attenuation spectra over three measurements of pigments a) PY74, b) PY65, c) PR122, d) PR170 and e) PW6 dissolved in water, normalized to its concentration per gram of water and the optical properties of the pigments in Epoxy, measured by Duco and Alec (2023)[15]*

10.3 APPENDIX C: THE LOCATIONS OF THE TCB-MEASUREMENTS PER PHANTOM

Figure 22: *The locations for TcB-measurements for phantom 1 (top left) to phantom 6 (bottem right), from left to right.*

10.4 APPENDIX D: MEASURED ATTENUATION SPECTRA OF THE INDIVIDUAL PIGMENTS

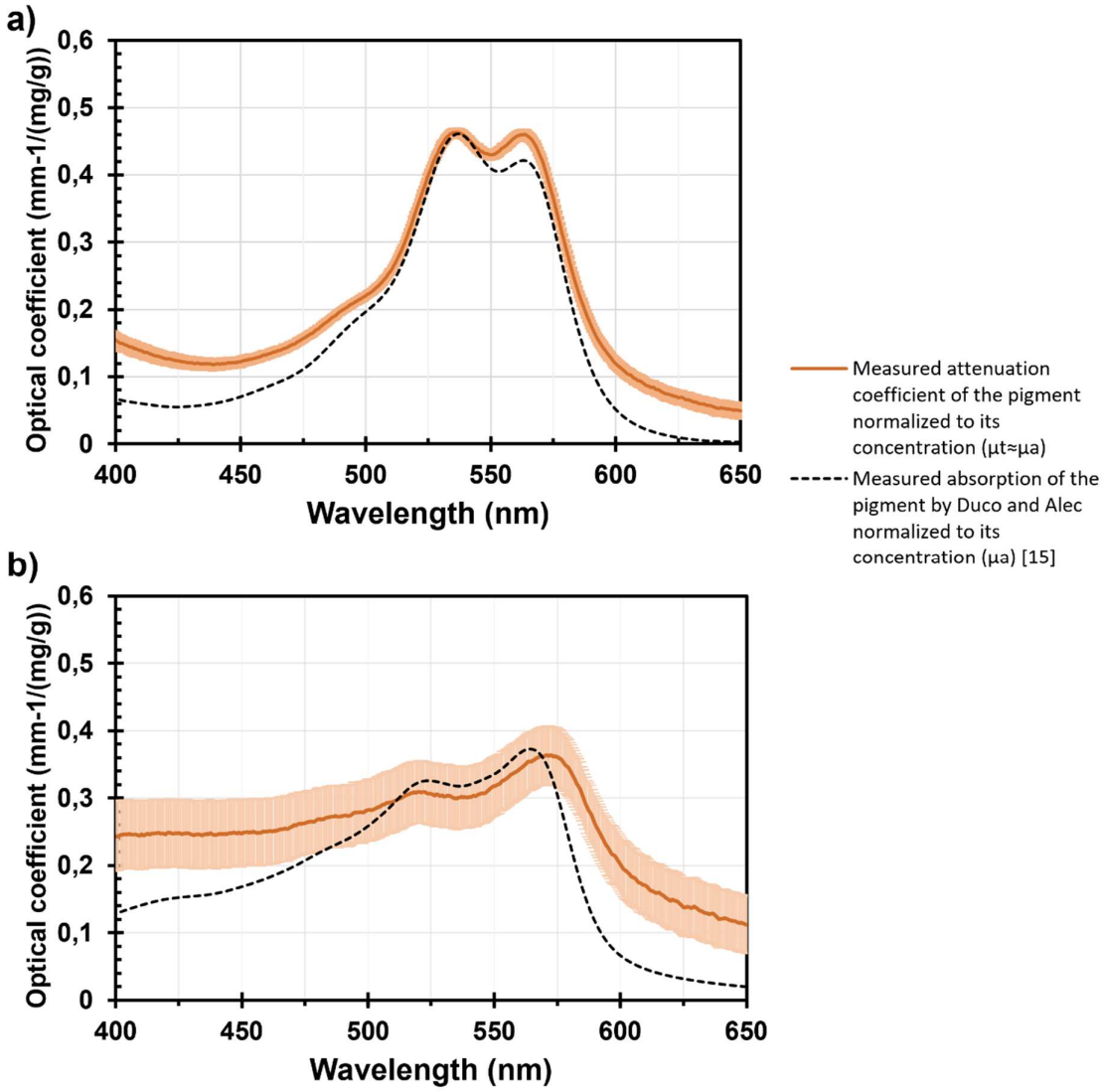

Figure 23: *The averaged attenuation spectrum over 5 measurements, from this study with standard deviation and absorption spectrum adapted from Duco and Alec (2023)[15] for pigment PR122 (a) and pigment PR170 (b), against the wavelength range of 400-650 nm.*

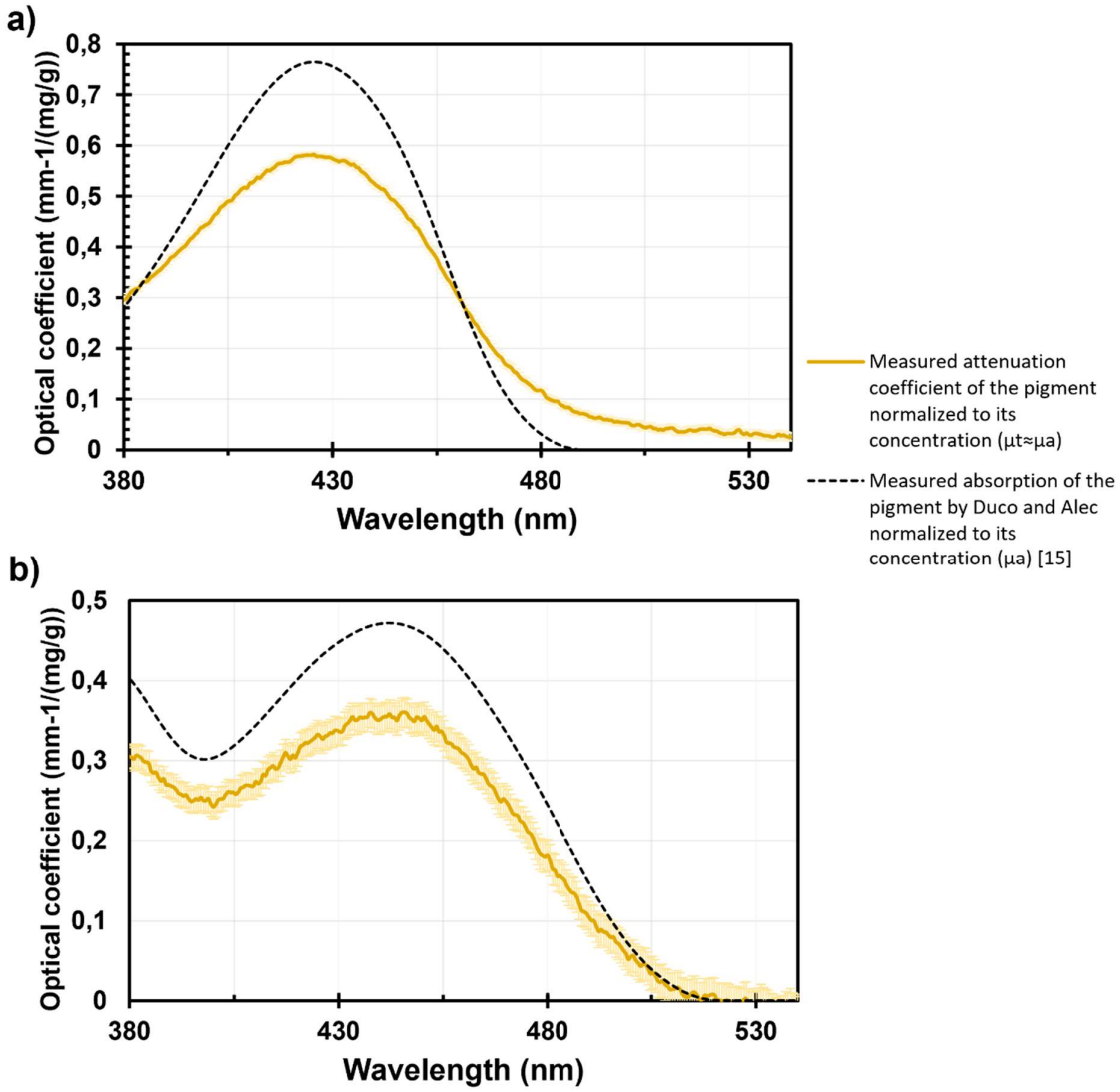

Figure 24: *The averaged attenuation spectrum over 5 measurements, from this study with standard deviation and absorption spectrum adapted from Duco and Alec (2023)*[15] *for pigment PY74 (a) and pigment PY65 (b), against the wavelength range of 380-540 nm.*

10.5 APPENDIX E: COMPOSITION OF THE FABRICATED PHANTOMS

10.5.1 Appendix E1: Measured quantities of pigment and epoxy per phantom

Phantom	Pigment	Quantity of pigment (mg)	Quantity Epoxy A	Quantity Epoxy B
1	PY74	44,4	24,95	22,42
	PR122	35,4		
	PW6	203,5		
2	PY74	179,3	25,08	22,73
	PR122	35,5		
	PW6	203,4		
3	PY74	192	24,91	22,57
	PR122	35,2		
	PW6	203,4		
4	PY74	286,7	25,03	22,51
	PR122	35,4		
	PW6	264,6		
5	PY74	478	25,11	22,55
	PR122	35,6		
	PW6	264,7		
6	PY74	189,9	25,00	22,49
	PR122	35,6		
	PW6	264,6		

10.5.2 Appendix E2: Calculated concentration of the phantoms and fabricated thin layers

Phantom		Concentration of the phantom	Concentration of the thin layer
1	Scattering agents	4,21	4,29
	Absorbing agents	1,74	1,68
2	Scattering agents	4,12	4,25
	Absorbing agents	4,48	4,49
3	Scattering agents	4,19	4,28
	Absorbing agents	4,67	4,79
4	Scattering agents	5,58	5,57
	Absorbing agents	6,78	6,78
5	Scattering agents	5,55	5,55
	Absorbing agents	10,50	10,78
6	Scattering agents	5,56	5,57
	Absorbing agents	4,76	4,74

10.6 Appendix F: TcB datasets for the Phantoms

Phantom 1, without ultrasound gel, with Tegaderm

Location	1	2	3	4	5	Total
Average	5,6	0	0	1,4	0	1,40
Standard deviation	6,7	0	0	1,4	0	3,7
Range	15	0	0	7	0	15
Number of measurements	10	10	10	10	10	50

Location	1	2	3	4	5
Measurement 1	15	0	0	0	0
Measurement 2	0	0	0	7	0
Measurement 3	3	0	0	0	0
Measurement 4	10	0	0	0	0
Measurement 5	0	0	0	0	0

Phantom 2, without ultrasound gel, with Tegaderm, first data set

Location	1	2	3	4	5	Total
Average	83	101,3	111	85,2	150,8	106,3
Standard deviation	30,1	45,6	63,6	22,8	99,2	57,9
Range	79	0	0	7	0	238
Number of measurements	10	10	10	10	10	50

Location	1	2	3	4	5
Measurement 1	51	68	130	74	92
Measurement 2	101	89	107	187	67
Measurement 3	52	61	125	211	106
Measurement 4	76	95	113	90	52
Measurement 5	92	95	289	57	221

Phantom 2, without ultrasound gel, with Tegaderm, second data set

Location	1	2	3	4	5	Total
Average	57,8	59	57,2	59,2	58	58,24
Standard deviation	2,2	10,3	8,2	17,8	11	10,0
Range	5	25	21	41	29	45
Number of measurements	5	5	5	5	5	25

Location	1	2	3	4	5
Measurement 1	56	59	55	60	59
Measurement 2	50	75	58	62	50
Measurement 3	52	61	48	56	69
Measurement 4	91	53	50	51	51
Measurement 5	52	46	61	56	75

Phantom 2, with ultrasound gel, with Tegaderm

Location	1	2	3	Total
Average	135,2	110	102,8	116
Standard deviation	34,3	22,2	28,3	29,2
Range	90	46	70	101
Number of measurements	5	5	5	15

Location	1	2	3	4	5
Measurement 1	120	140	86	154	176
Measurement 2	131	125	85	122	87
Measurement 3	103	75	112	79	145

Phantom 3, without ultrasound gel, with Tegaderm

Location	1	2	3	4	5	Total
Average	63	73,6	69	66,6	71,8	68,8
Standard deviation	2,2	9,0	17,7	12,5	15,8	11,96
Range	6	23	40	32	37	45
Number of measurements	10	10	10	10	10	50

Location	1	2	3	4	5
Measurement 1	63	60	64	62	66
Measurement 2	76	88	69	65	70
Measurement 3	80	95	57	58	55
Measurement 4	55	69	87	62	60
Measurement 5	67	64	63	65	100

Phantom 4, without ultrasound gel, with Tegaderm

Location	1	2	3	4	5	Total
Average	73,8	72,5	78,5	84,2	72,7	76,3
Standard deviation	15,0	7,9	9,9	18,8	6,2	12,3
Range	39	18	22	49	14	57
Number of measurements	10	10	10	10	10	50

Location	1	2	3	4	5
Measurement 1	64	75	103	65	64
Measurement 2	70	67	81	84	66
Measurement 3	75	72	71	89	93
Measurement 4	86	72	73	74	121
Measurement 5	82	69	79	69	69

Phantom 5 without ultrasound gel, with Tegaderm

Location	1	2	3	4	5	Total
Average	93	123	80,6	99,2	81	95,4
Standard deviation	27	66,5	2	34,3	10,8	35,6
Range	63	163	4	93	25	166
Number of measurements	10	10	10	10	10	50

Location	1	2	3	4	5
Measurement 1	141	80	80	78	86
Measurement 2	75	81	117	104	238
Measurement 3	82	82	79	82	78
Measurement 4	73	79	101	166	82
Measurement 5	94	76	73	72	97

Phantom 5 with ultrasound gel, with Tegaderm

Location	1	2	3	Total
Average	213	121	170,4	168,1
Standard deviation	72,8	20,1	45,9	61,2
Range	182	56	117	195
Number of measurements	5	5	5	15

Location	1	2	3	4	5
Measurement 1	107	172	250	247	289
Measurement 2	126	119	116	94	150
Measurement 3	100	161	205	169	217

Phantom 6 without ultrasound gel, with Tegaderm

Location	1	2	3	4	5	Total
Average	52	66,8	52,6	52	50	54,7
Standard deviation	1,9	8,3	3,1	4,7	0,8	7,4
Range	5	20	8	13	2	33
Number of measurements	10	10	10	10	10	50

Location	1	2	3	4	5
Measurement 1	51	50	52	55	52
Measurement 2	59	69	79	68	59
Measurement 3	52	55	52	56	48
Measurement 4	46	59	49	51	56
Measurement 5	51	49	50	50	51

Phantom 6 without ultrasound gel, without Tegaderm

Location	1	2	3	4	5	Total
Average	85,2	67,4	68,6	73,8	70,2	73
Standard deviation	9,4	8,8	4,6	8,8	7,4	9,8
Range	21	23	11	22	19	43
Number of measurements	5	5	5	5	5	25

Location	1	2	3	4	5
Measurement 1	79	91	99	78	79
Measurement 2	56	71	69	62	79
Measurement 3	65	69	63	72	74
Measurement 4	89	71	73	67	69
Measurement 5	83	67	69	64	68

Phantom 6 without ultrasound gel, without Tegaderm, measured on the other side of the phantom

Location	1	2	3	Total
Average	43	47,6	43	44,5
Standard deviation	5,2	4,0	5,3	4,9
Range	13	11	13	19
Number of measurements	5	5	5	15

Location	1	2	3	4	5
Measurement 1	47	44	46	34	44
Measurement 2	42	46	53	48	49
Measurement 3	52	39	43	39	42

Phantom 6 with ultrasound gel, with Tegaderm

Location	1	2	3	Total
Average	166,4	151	148,2	155,2
Standard deviation	19,7	13,1	22,6	18,7
Range	48	34	57	84
Number of measurements	5	5	5	15

Location	1	2	3	4	5
Measurement 1	153	170	199	159	151
Measurement 2	171	154	142	151	137
Measurement 3	165	172	139	115	150